AD-A085 743 SPERRY RESEARCH CENTER SUDBURY MA F/G 20/3
SPACE-TIME INTEGRAL EQUATION APPROACH TO DIELECTRIC TARGETS.(U)
MAR 80 C L BENNETT, H MIERAS, R LYONS F30602-79-C-0060
UNCLASSIFIED SRC-CR-79-81 RADC-TR-79-356 NL

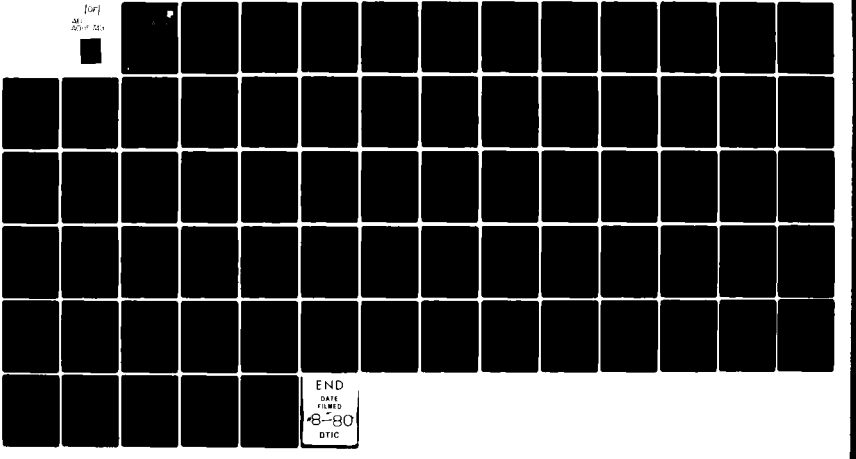

END
DATE FILMED
8-80
DTIC

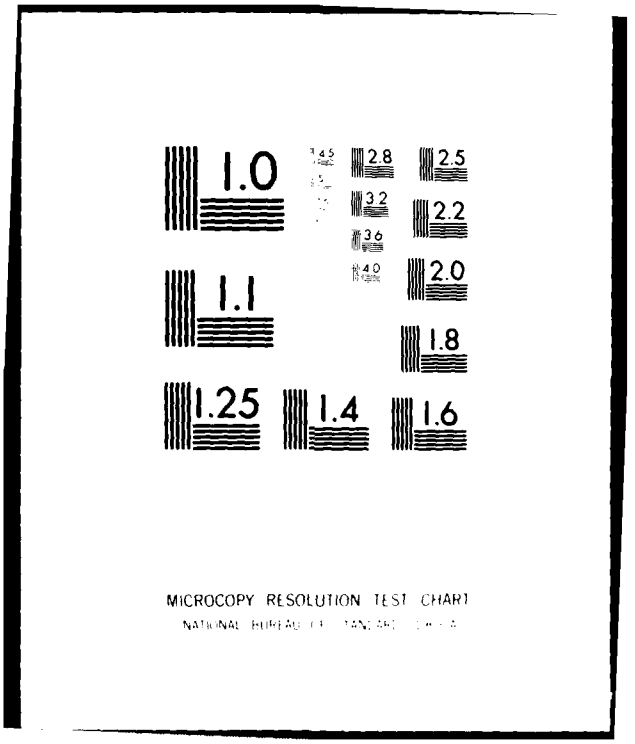
1.0
2.8
2.5
3.2
2.2
3.6
2.0
1.1
1.8
1.25
1.4
1.6
MICROCOPY RESOLUTION TEST CHART

RADC-TR-79-356
Final Technical Report
March 1980

LEVEL II

SPACE-TIME INTEGRAL EQUATION APPROACH TO DIELECTRIC TARGETS

Sperry Research Center

C. L. Bennett
H. Mieras
R. Lyons

ROME AIR DEVELOPMENT CENTER
Air Force Systems Command
Griffiss Air Force Base, New York 13441

This report has been reviewed by the RADC Public Affairs Office (PA) and is releasable to the National Technical Information Service (NTIS). At NTIS it will be releasable to the general public, including foreign nations.

RADC-TR-79-356 has been reviewed and is approved for publication.

APPROVED:

DANIEL L. TAURONEY
Project Engineer

APPROVED:

FRANK J. REHM
Technical Director
Surveillance Division

FOR THE COMMANDER:

JOHN P. HUSS
Acting Chief, Plans Office

If your address has changed or if you wish to be removed from the RADC mailing list, or if the addressee is no longer employed by your organization, please notify RADC (OCTM), Griffiss AFB NY 13441. This will assist us in maintaining a current mailing list.

Do not return this copy. Retain or destroy.

UNCLASSIFIED

SECURITY CLASSIFICATION OF THIS PAGE (When Data Entered)

REPORT DOCUMENTATION PAGE

READ INSTRUCTIONS BEFORE COMPLETING FORM

1. REPORT NUMBER: RADC-TR-79-356	2. GOVT ACCESSION NO.: AD-A085 743
3. RECIPIENT'S CATALOG NUMBER:	
4. TITLE (and Subtitle): SPACE-TIME INTEGRAL EQUATION APPROACH TO DIELECTRIC TARGETS	5. TYPE OF REPORT & PERIOD COVERED: Final Technical Report, 1 Jan [redacted] 30 Sep 79
	6. PERFORMING ORG. REPORT NUMBER: SRC-CR-79-81
7. AUTHOR(s): C. L. Bennett, H. Mieras, R. Lyons	8. CONTRACT OR GRANT NUMBER(s): F30602-79-C-0060
9. PERFORMING ORGANIZATION NAME AND ADDRESS: Sperry Research Center, 100 North Road, Sudbury MA 01776	10. PROGRAM ELEMENT, PROJECT, TASK AREA & WORK UNIT NUMBERS: 62702F, 45061339, 13
11. CONTROLLING OFFICE NAME AND ADDRESS: Rome Air Development Center (OCTM), Griffiss AFB NY 13441	12. REPORT DATE: Mar [redacted] 80
	13. NUMBER OF PAGES: 73
14. MONITORING AGENCY NAME & ADDRESS(if different from Controlling Office): Same	15. SECURITY CLASS. (of this report): UNCLASSIFIED
	15a. DECLASSIFICATION/DOWNGRADING SCHEDULE: N/A

16. DISTRIBUTION STATEMENT (of this Report)

Approved for public release; distribution unlimited.

17. DISTRIBUTION STATEMENT (of the abstract entered in Block 20, if different from Report)

Same

18. SUPPLEMENTARY NOTES

RADC Project Engineer: Daniel L. Tauroney (OCTM)

19. KEY WORDS (Continue on reverse side if necessary and identify by block number)

Space-Time Integral Equation
Scattering
Dielectric Solids
Numerical Techniques
Frequency Domain
Time Domain

20. ABSTRACT (Continue on reverse side if necessary and identify by block number)

This report describes the extension of the space-time integral equation approach to scattering from dielectric solids. The theory of the space-time integral equation approach is presented and verified by comparison with the classical solution for scattering from a sphere. The technique and solution for scattering from a complex target consisting of wings on a fuselage are presented based on a model closely resembling a Tomahawk missile. Experimental verification of the calculations is pro-

(Cont'd)

DD FORM 1 JAN 73 1473 EDITION OF 1 NOV 65 IS OBSOLETE

UNCLASSIFIED

SECURITY CLASSIFICATION OF THIS PAGE (When Data Entered)

405 199

Item 20 (Cont'd)

vided by time domain scattering range response measuremnts on a variety of targets.

TABLE OF CONTENTS

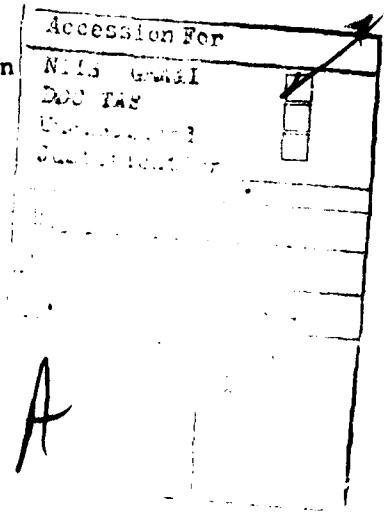

LIST OF ILLUSTRATIONS

EVALUATION

This report is another building block in the solution for the transient response of either a metallic or dielectric targets. These solutions will provide data over the entire frequency spectrum and will reduce the need for extensive measurement programs. The computation of the response of a Tomahawk like target will be useful in cruise missile detection and identification systems. This effort has application to TPO^RlC Surveillance Sensor Techniques.

DANIEL L. TAURONEY
Project Engineer

SECTION I
INTRODUCTION

This is the final report under Contract No. F30602-79-C-0060.

The main result is the application of the space-time integral equation approach to the dielectric scattering problem. The response of dielectrics is of recent renewed interest due to the potential use of radar absorbing material (RAM) on radar targets. The classical frequency domain solution was given for the sphere by Mie in 1906 (see, for example ref. [1]). Modern computing power makes short work of such a solution; see for example the extension of the Mie result to layered spherical shells in ref. [2]. In recent years, numerical techniques have been brought out to free the problem from the constraints of the separable coordinate system imposed by the classical solution. Most of these techniques are applied in the frequency domain: Mautz and Harrington [3] investigated a frequency domain solution using surface integral equations on solids with axial symmetry. A time domain solution is presented in [4] for complex dielectrics, with simplified geometries. The time domain integral equation approach has been pursued at the Sperry Research Center for a number of years [5,6]. Results have been obtained for conducting solids, conducting plates and compound targets. These computations have been verified by measurement on the time domain scattering range. In the present effort these techniques are directly extended to dielectric solids.

In Section 2 the theory of the space-time integral equation approach is presented. The numerical implementation is detailed and results are given for several shapes. The response of the sphere, in comparison with the classical solution, is used as one aspect of the verification of the technique.

In Section 3 the technique and solution is given for scattering from a complex target consisting of wings on a fuselage. A model closely resembling a Tomahawk missile is used.

The calculations are verified by measurement on the scattering range. The scattering range and results of response measurements on a variety of targets are described in Section 4.

SECTION II

SPACE TIME INTEGRAL EQUATION SOLUTION FOR SCATTERING FROM DIELECTRIC SOLIDS

2.1 THEORY

Consider a closed surface S separating a uniform exterior (ϵ, μ, c) from a uniform dielectric interior with $\epsilon_1 = \epsilon_r \epsilon$, $\mu_1 = \mu_r \mu$, and $c_1 = c/\sqrt{\epsilon_r \mu_r}$ as shown in Figure 2-1. In the time domain, the exterior electromagnetic field can be written in terms of its retarded values on S, a form known as the Kirchhoff integral representation.

$$\vec{H}(\vec{r},t) = \vec{H}^i(\vec{r},t) + \frac{1}{4\pi} \oint \left\{ \frac{1}{R} \hat{n}' \times \sqrt{\frac{\epsilon}{\mu}} \frac{\partial \vec{E}'}{c\partial t} + L\left((\hat{n}' \cdot \vec{H}')\hat{R} + (\hat{n}' \times \vec{H}') \times \hat{R}\right) \right\} dS' \tag{2-1}$$

$$\vec{E}(\vec{r},t) = \vec{E}^i(\vec{r},t) + \frac{1}{4\pi} \oint \left\{ -\frac{1}{R} \hat{n}' \times \sqrt{\frac{\mu}{\epsilon}} \frac{\partial \vec{H}'}{c\partial t} + L\left((\hat{n}' \cdot \vec{E}')\hat{R} + (\hat{n}' \times \vec{E}') \times \hat{R}\right) \right\} dS' \tag{2-2}$$

where

$\vec{E}'$ means $\vec{E}(\vec{r}',\tau)$, etc.

$\tau = t - R/c$

R is the magnitude of $\vec{R} = \vec{r} - \vec{r}'$

$\hat{R}$ is the unit direction of $\vec{R}$

$L = \frac{1}{R^2} + \frac{1}{Rc} \frac{\partial}{\partial \tau}$

$\hat{n}'$ is the outward normal at $\vec{r}'$

These equations are derived using the Green's theorem with the time domain Green's function $G(\vec{r},\vec{r}'|t,\tau) = 1/R\ \delta(t - R/c - \tau)$ and making use only of the source-free Maxwell's equations

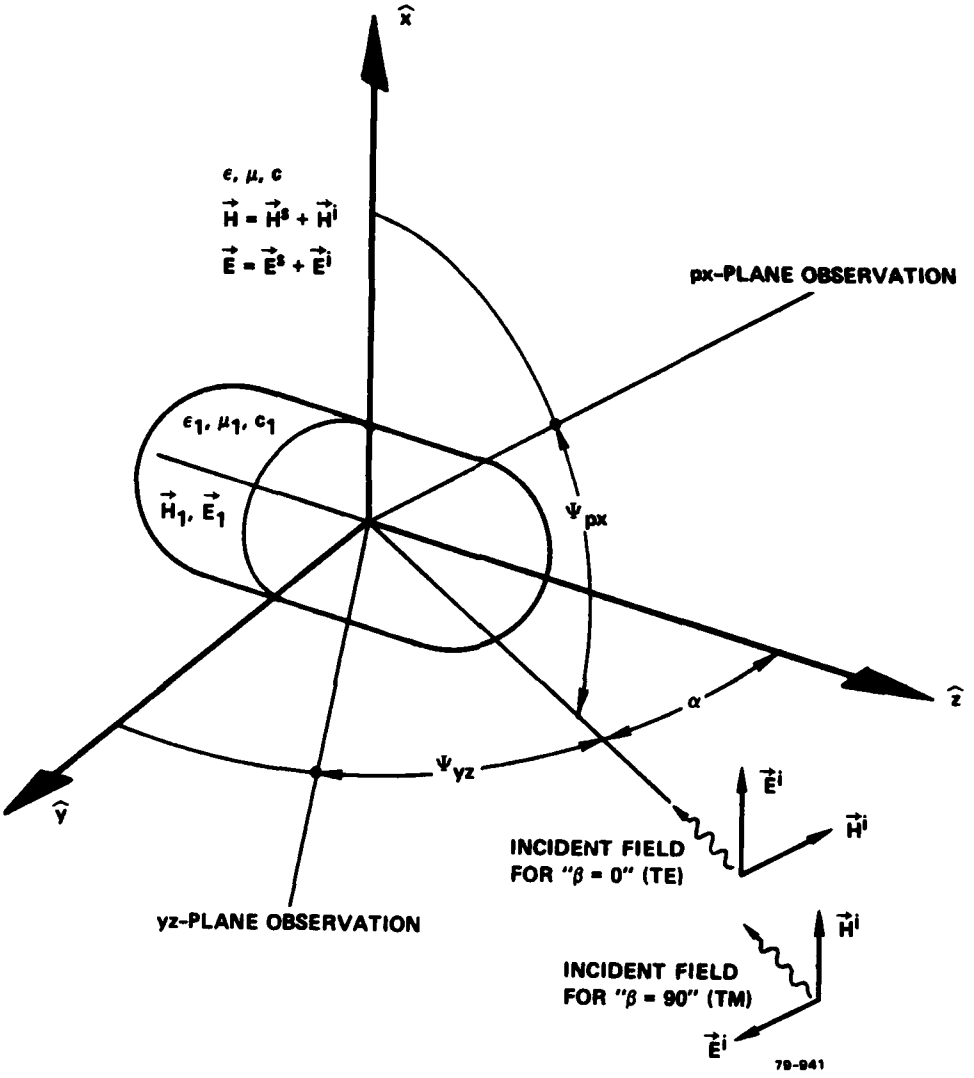

FIG. 2-1 Scattering problem geometry.

$$\nabla \times \vec{E} = - \sqrt{\frac{\mu}{\epsilon}} \frac{\partial \vec{H}}{c \partial t} ,$$

$$\nabla \times \vec{H} = \sqrt{\frac{\epsilon}{\mu}} \frac{\partial \vec{E}}{c \partial t}$$

$$\nabla \cdot \vec{E} = 0 , \nabla \cdot \vec{H} = 0 .$$

A readable derivation in the frequency domain is given by Jackson [7]. The external sources are represented by $\vec{H}^i$ and $\vec{E}^i$ (the incident field). A similar pair of integral equations can be written for the interior fields $\vec{H}_1$ and $\vec{E}_1$. But inside there is no incident field and the sign of the integral is changed as $\hat{n}$ remains pointing outward:

$$\vec{H}_1(\vec{r},t) = - \frac{1}{4\pi} \oint \left\{ \frac{1}{R} \hat{n}' \times \sqrt{\frac{\epsilon_1}{\mu_1}} \frac{\partial \vec{E}_1''}{c_1 \partial t} + L_1 \left(\left(\hat{n}' \cdot \vec{H}_1'' \right) \hat{R} + \left(\hat{n}' \times \vec{H}_1'' \right) \times \hat{R} \right) \right\} dS' \tag{2-3}$$

$$\vec{E}_1(\vec{r},t) = - \frac{1}{4\pi} \oint \left\{ - \frac{1}{R} \hat{n}' \times \sqrt{\frac{\mu_1}{\epsilon_1}} \frac{\partial \vec{H}_1''}{c_1 \partial t} + L_1 \left(\left(\hat{n}' \cdot \vec{E}_1'' \right) \hat{R} + \left(\hat{n}' \times \vec{E}_1'' \right) \times \hat{R} \right) \right\} dS' \tag{2-4}$$

for $\vec{r}$ inside,

where

$$\vec{E}_1'' \text{ means } \vec{E}_1\left(\vec{r}', \tau_1\right)$$

$$\tau_1 = t - R/c_1$$

$$L_1 = \frac{1}{R^2} + \frac{1}{Rc_1} \frac{\partial}{\partial t} .$$

The double prime is used to emphasize that the retardation is at speed c_1. These equations permit the calculation of the field, in particular the far-scattered field, from the surface quantities once these are known. Our problem is to solve the equations on the surface.

For $\vec{r}$ on S the term with the operator L in each of the integrals is singular. This singularity can be removed in the following way: consider equation (2-1). We note that the integral takes on the same value, if the singular point is excluded, whether $\vec{r}$ is just inside or just outside of S. However, the singular part changes sign as $\vec{r}$ passes through S. We now require that equation (2-1) have value zero evaluated inside S. That is,

$$\vec{H}(\vec{r} \in S^+) = \vec{H}^i + \vec{I}_{NS} + \vec{I}_S$$

$$0 = \vec{H}(\vec{r} \in S^-) = \vec{H}^i + \vec{I}_{NS} - I_S \ .$$

Adding, we get

$$\vec{H}(\vec{r} \in S) = 2\vec{H}^i + 2\vec{I}_{NS} \tag{2-5}$$

Here, I_{NS} is the integral with the nonsingular point removed; usually written as $\mathcal{f} \ldots dS'$. A similar argument is made with equation (2-3), where now $\vec{H}_1(\vec{r} \in S^+) = 0$. *This is no more than a restatement of the properties of a* Green's function solution to a boundary value problem. The discontinuity at the boundary S is then required to be expressed by the known physical boundary conditions. These boundary conditions are

$$\hat{n} \times \vec{H}_1 = \hat{n} \times \vec{H} \equiv \vec{J} \tag{2-6}$$

$$\vec{E}_1 \times \hat{n} = \vec{E} \times \hat{n} \equiv \vec{M} \tag{2-7}$$

$$\mu_r\left(\hat{n} \cdot \vec{H}_1\right) = \hat{n} \cdot \vec{H} \equiv H_n \tag{2-8}$$

$$\varepsilon_r\left(\hat{n} \cdot \vec{E}_1\right) = \hat{n} \cdot \vec{E} \equiv E_n \tag{2-9}$$

The first of these boundary conditions also serve to define the tangential electric and magnetic surface currents. (Also one could define the surface charges $\sigma = \vec{E} \cdot \hat{n}$ and $\sigma_m = \vec{H} \cdot \hat{n}$, but here we will prefer to write E_n and H_n.) For convenience, we will also normalize the exterior constants $\varepsilon = \mu = c = 1$ so that

$$\sqrt{\frac{\epsilon_1}{\mu_1}}\,\frac{1}{c_1} = \epsilon_r\left(\sqrt{\frac{\epsilon}{\mu}}\,\frac{1}{c}\right) = \epsilon_r$$

and (2-10)

$$\sqrt{\frac{\mu_1}{\epsilon_1}}\,\frac{1}{c_1} = \mu_r\left(\sqrt{\frac{\mu}{\epsilon}}\,\frac{1}{c}\right) = \mu_r$$

With these simplifications and application of equation (2-5) and the boundary conditions, we obtain the following set of equations for $\vec{r}$ on S:

$$\vec{J}(\vec{r},t) = \hat{n} \times \vec{H} = 2\,\vec{J}^{i} + \hat{n} \times \frac{1}{2\pi} \oint \left\{ -\frac{1}{R}\frac{\partial \vec{M}'}{\partial t} + L\left(H_n' \hat{R} + \vec{J}' \times \hat{R}\right)\right\} dS' \qquad (2\text{-}11)$$

$$\vec{J}(\vec{r},t) = \hat{n} \times \vec{H}_1 = -\hat{n} \times \frac{1}{2\pi} \oint \left\{ -\frac{\epsilon_r}{R}\frac{\partial \vec{M}''}{\partial t} + L_1\left(\frac{H_n''}{\mu_r}\hat{R} + \vec{J}'' \times \hat{R}\right)\right\} dS' \qquad (2\text{-}12)$$

$$\vec{M}(\vec{r},t) = -\hat{n} \times \vec{E} = 2\,\vec{M}^{i} - \hat{n} \times \frac{1}{2\pi} \oint \left\{ -\frac{1}{R}\frac{\partial \vec{J}'}{\partial t} + L\left(E_n' \hat{R} - \vec{M}' \times \hat{R}\right)\right\} dS' \qquad (2\text{-}13)$$

$$\vec{M}(\vec{r},t) = -\hat{n} \times \vec{E}_1 = \hat{n} \times \frac{1}{2\pi} \oint \left\{ -\frac{\mu_r}{R}\frac{\partial J''}{\partial t} + L_1\left(\frac{E_n''}{\epsilon_r}\hat{R} - \vec{M}'' \times \hat{R}\right)\right\} dS' \qquad (2\text{-}14)$$

The above are for the tangential components. For the normal components we can write:

$$H_n = 2H_n^{i} + \hat{n} \cdot \frac{1}{2\pi} \oint \left\{ \ldots \text{ as in 2-11 } \ldots \right\} dS' \qquad (2\text{-}15)$$

$$\frac{H_n}{\mu_r} = -\hat{n} \cdot \frac{1}{2\pi} \oint \left\{ \ldots \text{ as in 2-12 } \ldots \right\} dS' \qquad (2\text{-}16)$$

$$E_n = 2E_n^{i} + \hat{n} \cdot \frac{1}{2\pi} \oint \left\{ \ldots \text{ as in 2-13 } \ldots \right\} dS' \qquad (2\text{-}17)$$

$$\frac{E_n}{\epsilon_r} = -\hat{n} \cdot \frac{1}{2\pi} \oint \left\{ \ldots \text{ as in 2-14 } \ldots \right\} dS' \qquad (2\text{-}18)$$

where $\vec{J}^i \equiv \hat{n} \times \vec{H}^i(\vec{r},t)$ and similarly for $\vec{M}^i$, E_n^i, M_n^i .

Several observations are in order. First, (2-11) through (2-18) are too many equations. The field vectors $\vec{E}$ and $\vec{H}$ are not independent but related through the Maxwell equations. Hence equations (2-11) and (2-12) for the surface components of $\vec{H}$ and equation (2-13) for the normal component of $\vec{H}$ are sufficient to solve the problem. Such a formulation is detailed in Appendix 7.1. This approach led to instabilities in the numerical solution and was abandoned. Second, it is known that only the tangential components of $\vec{E}$ and $\vec{H}$, that is $\vec{J}$ and $\vec{M}$, are required to completely specify the field. The normal components can be eliminated by means of the continuity relations

$$\nabla_s \cdot \vec{J} + \frac{\partial}{\partial t}\left(E_n - E_{ln}\right) = 0 \ ,$$

$$\nabla_s \cdot \vec{M} + \frac{\partial}{\partial t}\left(H_n - H_{ln}\right) = 0 \ . \qquad (2\text{-}19)$$

The operator $\nabla_s \cdot$ is the surface divergence. The numerical evaluation of $\nabla_s \cdot \vec{J}$ on an arbitrary three dimensional surface can be very inaccurate. For that reason, the explicit determination of the normal components (equations (2-15) through (2-18)) was retained. There was, at the outset, some worry that the direct evaluation of H_n and E_n, without application of the constraints (2-19), would lead to instabilities in the time domain solution. However, the present formulation appears to be successful.

Since we wish to retain the complete formulation of equations (2-11) through (2-18), we need to combine these somehow into fewer equations such as to permit the unique solution for the six scalar components of $\vec{J}$, $\vec{M}$, H_n, E_n. We achieve this, using a general technique, similar to that described by Mautz and Harrington [3]. Namely, multiply the second of the $\vec{H}$ (or $\vec{J}$) equations by β and add to the first; multiply the second of the $\vec{E}$ (or $\vec{M}$) equations by α and add to the first. For example, from (2-15), (2-16) we obtain

$$H_n + \frac{\underset{\sim}{\beta}}{\mu_r} H_n = 2H_n^i + \hat{n} \cdot \left[\frac{1}{2\pi} \int \left\{ \ldots \text{ as in 2-11 } \ldots \right\} dS' \right.$$

$$\left. - \frac{\underset{\sim}{\beta}}{2\pi} \int \left\{ \ldots \text{ as in 2-12 } \ldots \right\} dS' \right].$$

Mautz and Harrington showed that the solution obtained is unique if $\underset{\sim}{\alpha}$, $\underset{\sim}{\beta}$ satisfy $\underset{\sim}{\alpha}\,\underset{\sim}{\beta}^*$ = positive real. Their formulation was in the frequency domain. In the time domain, complex $\underset{\sim}{\alpha}$ means $\underset{\sim}{\alpha} = \alpha_1 + \alpha_2\, \partial/\partial t$. The above requirement thus becomes that, for

$$\underset{\sim}{\alpha} = \alpha_1 + \alpha_2 \frac{\partial}{\partial t}$$

$$\underset{\sim}{\beta} = \beta_1 + \beta_2 \frac{\partial}{\partial t} ,$$

the conditions $\beta_1\alpha_2 - \alpha_1\beta_2 = 0$ and $\alpha_1\beta_1 > \alpha_2\beta_2$ guarantee uniqueness. It is likely that other non-zero values of $\underset{\sim}{\alpha}$, $\underset{\sim}{\beta}$ will also lead to unique solutions. Here, we will use the simpler form of the constants $\underset{\sim}{\alpha} = \alpha_1$ and $\underset{\sim}{\beta} = \beta_1$.

The solution is now formally complete. To solve the scattering problem, we first solve the problem for all time on the surface. This last can be done by a simple marching in time procedure since the quantities appearing inside the integrals need to be evaluated at the retarded times τ and τ_1. If it is arranged that τ and τ_1 are always at least one numerical time step earlier than the current time, then no matrix inversion needs to be performed. To get started, the incident pulse is taken as the time and bandlimited function

$$|\vec{H}^i(t)| = \frac{a_n}{\sqrt{\pi}}\, e^{-(a_n t)^2} \qquad (2\text{-}20)$$

The process is started at a time sufficiently early for the above to be considered zero.

Having completed the surface calculation, the far field can then be computed quickly for the backscatter case as well as at any number of

bistatic angles, by a limiting form of equation (2-1) or (2-2). As $r \to \infty$, the scattered field is given by

$$r \vec{H}^s\left(\vec{r}, t_f\right) = \frac{1}{4\pi} \oint \left\{ - \frac{\partial \vec{M}'}{\partial t} + \frac{\partial \vec{J}'}{\partial t} \times \hat{r} \right\} dS' \qquad (2\text{-}21)$$

where

$$\vec{J}' = \vec{J}(\vec{r}', t')$$

$$t' = t_f + \vec{r}' \cdot \hat{r} \ .$$

The far field time t_f is referenced to $t = 0$ and the origin. (That is, an impulse reflected from the origin at $t = 0$ arrives in the far field at $t_f = 0$.)

Note that since $\vec{H}^s$ must be perpendicular to $\hat{r}$, the integral of $\frac{\partial \vec{M}}{\partial t} \cdot \hat{r}$ over the closed surface S must vanish. Hence $\partial \vec{M}/\partial t$ may be replaced by $(\hat{r} \times \partial \vec{M}/\partial t) \times \hat{r}$ in the equation. This observation is useful when determining the relative importance of different regions of S and for debugging purposes.

2.2 NUMERICAL IMPLEMENTATION

The surface S is divided into patches of approximately equal size, with sample points at their centers. Time also is quantized. The values of $\vec{J}$ and $\partial \vec{J}/\partial t$, etc., are assumed to be constant over a patch. In evaluating the integrals, the quantities $1/R$ and the operators $L\hat{R}$ are also assumed to be constant over the patch, except for the "self-patch". The self-patch (the patch containing both observation and integration points, $\vec{r} = \vec{r}'$) is integrated analytically. The result is removed from the integral, leaving the "non-self" integral.

The self-integrals are of three types. To evaluate these we consider each (curvilinear rectangular) self-patch with area ΔS as a circular patch with radius γ. Then the first of the self integrals is straightforward

$$\frac{1}{2\pi}\int_{\Delta S}\frac{dS}{R} = \sqrt{\frac{\overline{\Delta S}}{\pi}} = \gamma \ . \qquad (2\text{-}22)$$

The others require the expansion of $\hat{n}$ and $\hat{R}$ in surface coordinates. This is done in Appendix 7.3. The results are

$$\hat{n} \cdot \frac{1}{2\pi}\int_{\Delta S} L\, H_n'\, \hat{R}\, dS' = -\, e_s H_n \qquad (2\text{-}23)$$

with

$$e_s = \gamma\left(\frac{K_u + K_v}{4}\right) ;$$

and

$$\hat{n} \times \frac{1}{2\pi}\int_{\Delta S} L\, \vec{J}' \times \hat{R}\, dS = \overleftrightarrow{e} \cdot \vec{J}$$

The dyadic $\overleftrightarrow{e}$ is no more than a convenient short-hand for the result, which is polarization dependent. The magnitude of $\overleftrightarrow{e}$ is

$$e = \frac{\gamma}{4}\left(K_u - K_v\right) \ , \qquad (2\text{-}24)$$

where K_u and K_v are the principal curvatures, and

$$\overleftrightarrow{e} = e\left[\hat{a}_u\hat{a}_u - \hat{a}_v\hat{a}_v\right] ,$$

so that

$$\overleftrightarrow{e} \cdot \vec{J} = e\,\hat{a}_u J_u - e\,\hat{a}_v J_v \ .$$

Note that $e = 0$ for a sphere.

The standard geometry identifies $(\hat{a}_u, \hat{a}_v, \hat{n})$ as $(\hat{\theta}, \hat{\phi}, \hat{r})$ for the sphere. For a body of revolution about the z-axis, $\hat{a}_u$ becomes the tangent $\hat{t}$ almost parallel to $\hat{\theta}$: $(\hat{t}, \hat{\phi}, \hat{n})$. Hence, for a cylinder of radius a,

we have on the cylinder body, $K_u = 0$, $K_v = -1/a$, so that $e = \frac{\gamma}{4}(1/a) > 0$, and $e_s = -\frac{\gamma}{4}(1/a) < 0$.

We will define and write out the numerical form of the non-self integrals explicitly. At time t_j, for observation point $\vec{r}_i$:

$$\vec{I}_{ij} = \sum_{k\neq i} \left\{ -\frac{1}{R_{ik}} \frac{\partial \vec{M}'_k}{\partial t} + L_{ik} H'_{n_k} \hat{R}_{ik} + L_{ik} \vec{J}'_k \times \hat{R}_{ik} \right\} \frac{\Delta S_k}{2\pi} \qquad (2\text{-}25)$$

$$\vec{I}_{1_{ij}} = \sum_{k\neq i} \left\{ -\frac{\epsilon_r}{R_{ik}} \frac{\partial \vec{M}''_k}{\partial t} + L_{1_{ik}} \frac{H''_{n_k}}{\mu_r} \hat{R}_{ik} + L_{1_{ik}} \vec{J}''_k \times \hat{R}_{ik} \right\} \frac{\Delta S_k}{2\pi} \qquad (2\text{-}26)$$

$$\vec{K}_{ij} = \sum_{k\neq i} \left\{ -\frac{1}{R_{ik}} \frac{\partial \vec{J}'_k}{\partial t} + L_{ik} E'_{n_k} \hat{R}_{ik} - L_{ik} \vec{M}'_k \times \hat{R}_{ik} \right\} \frac{\Delta S_k}{2\pi} \qquad (2\text{-}27)$$

$$\vec{K}_{1_{ij}} = \sum_{k\neq i} \left\{ -\frac{\mu_r}{R_{ik}} \frac{\partial \vec{J}''_k}{\partial t} + L_{1_{ik}} \frac{E''_{n_k}}{\epsilon_r} \hat{R}_{ik} - L_{1_{ik}} \vec{M}''_k \times \hat{R}_{ik} \right\} \frac{\Delta S_k}{2\pi} \qquad (2\text{-}28)$$

where $\vec{M}'_k$, etc., are evaluated at $\tau = t_j - R_{ik}$

$\vec{M}''_k$, etc., are evaluated at $\tau_1 = t_j - R_{ik}/c_r$.

At each time step t_j the above integrals are evaluated for each observation point i. To do this, it is required to keep past values of the six surface quantities in storage for all times back to $R_{max}/c_r + 3\Delta t$, where R_{max} is the greatest target diameter, and Δt is the time step. The evaluations at τ (or τ_1) are achieved by polynomial interpolation over values at the five time points nearest τ. (An alternate interpolation method, which performs smoothing on the five points, has also been used and has the advantage of suppressing instabilities, though at the expense of a somewhat reduced accuracy in the final result.)

For convenience in writing, we drop the subscripts i, j in the following. The numerical forms of equations (2-11) and (2-12) are thus

$$\left(\overleftrightarrow{I} - \overleftrightarrow{e}\right) \cdot \vec{J} + \gamma\, \hat{n} \times \frac{\partial \vec{M}}{\partial t} = 2\, \vec{J}^{i} + \hat{n} \times \vec{I}$$

$$\left(\overleftrightarrow{I} + \overleftrightarrow{e}\right) \cdot \vec{J} - \gamma \varepsilon_r\, \hat{n} \times \frac{\partial \vec{M}}{\partial t} = -\, \hat{n} \times \vec{I}_1 \qquad (2\text{-}29)$$

As described in Subsection 2.1, we will multiply the second of these by $\underset{\sim}{\beta}$ and add, obtaining

$$(1 + \underset{\sim}{\beta})\, \vec{\underset{\sim}{J}} + \gamma\left(1 - \varepsilon_r \underset{\sim}{\beta}\right)\, \hat{n} \times \frac{\partial \vec{M}}{\partial t} = 2\, \vec{J}^{i} + \hat{n} \times \left(\vec{I} - \underset{\sim}{\beta}\, \vec{I}_1\right) \qquad (2\text{-}30)$$

Here we have written $\vec{\underset{\sim}{J}}$ for convenience to mean

$$\vec{\underset{\sim}{J}} = \left[\overleftrightarrow{I} - \left(\frac{1 - \underset{\sim}{\beta}}{1 + \underset{\sim}{\beta}}\right) \overleftrightarrow{e}\right] \cdot \vec{J}\ ; \qquad (2\text{-}31)$$

for a sphere $\vec{\underset{\sim}{J}} = \vec{J}$; in any case this is a small correction factor.

The pair of $\vec{E}$ equations (2-13) and (2-14) will result in a similar form, but for $\vec{M}$ and $\hat{n} \times \partial\vec{J}/\partial t$. To solve simultaneously, we thus need to write a numerical form for the time derivative. Here we choose the first order form

$$\frac{\partial \vec{J}}{\partial t} = \left(\vec{J}\left(t_j\right) - \vec{J}\left(t_{j-1}\right)\right)/\Delta t\ . \qquad (2\text{-}32)$$

Since the constants γ, $\underset{\sim}{\alpha}$, $\underset{\sim}{\beta}$ will be such that the $\partial\vec{J}/\partial t$ and $\partial\vec{M}/\partial t$ terms are relatively small, the above approximation is good enough. For greater accuracy, however, one could use the second order form

$$\frac{\partial \vec{J}}{\partial t} = \left(1.5\, \vec{J}\left(t_j\right) - 2\, \vec{J}\left(t_{j-1}\right) + .5\, \vec{J}\left(t_{j-2}\right)\right)/\Delta t\ . \qquad (2\text{-}33)$$

We now multiply (2-14) by $\underset{\sim}{\alpha}$ and add to (2-13). Also, we will cross multiply the result by $\hat{n}$, in order to obtain the same unknowns. (Note that $(\hat{n} \times \vec{M}) \times \hat{n} = \vec{M}$, since $\vec{M}$ is a surface vector.) Also writing the time derivative numerically, we obtain the following pair of equations in unknowns

$\vec{J}$ and $\hat{n} \times \vec{M}$:

$$\left(1 + \underset{\sim}{\beta}\right) \vec{\underset{\sim}{J}} + \frac{\gamma}{\Delta t}\left(1 - \underset{\sim}{\beta}\,\underset{\sim}{\varepsilon}_r\right) \hat{n} \times \vec{M} = 2\,\vec{J}^{i} + \hat{n} \times \left(\vec{I} - \underset{\sim}{\beta}\,\vec{I}_1 + \frac{\gamma}{\Delta t}\left(1 - \underset{\sim}{\beta}\,\underset{\sim}{\varepsilon}_r\right) \vec{M}_{-1}\right)$$

$$\frac{\gamma}{\Delta t}\left(1 - \underset{\sim}{\alpha}\,\underset{\sim}{\mu}_r\right) \vec{J} + \left(1 + \underset{\sim}{\alpha}\right) \hat{n} \times \vec{M} = \hat{n} \times \left[2\vec{M}^{i} - \hat{n} \times \left(\vec{K} - \underset{\sim}{\alpha}\,\vec{K}_1 + \frac{\gamma}{\Delta t}\left(1 - \underset{\sim}{\alpha}\,\underset{\sim}{\mu}_r\right) \vec{J}_{-1}\right)\right] \tag{2-34}$$

The right-hand sides of these are just combinations of the integrals, already expressed in (2-25) through (2-28), with the incident field and the previous computed values. We can write these equations as

$$\begin{bmatrix} & \underset{\sim}{Q} & \end{bmatrix} \begin{bmatrix} \vec{\underset{\sim}{J}} \\ \\ \hat{n} \times \vec{\underset{\sim}{M}} \end{bmatrix} = \begin{bmatrix} \vec{V}_1 \\ \\ \vec{V}_2 \end{bmatrix} \tag{2-35}$$

and solve for each of the surface components u and v. [In the present computer program, the vectors are stored in Cartesian form, so that the equations are solved for the three Cartesian components. This introduces a slight complication, since $\vec{J}$ as well as $\vec{\underset{\sim}{J}}$ appears in the equation; this effect is neglected since it is small.] After solving for $\vec{\underset{\sim}{J}}$ and $\vec{\underset{\sim}{M}}$, the self-term correction dyadic is applied:

$$J_u = \underset{\sim}{J}_u \Big/ \left(1 - e\left(\frac{1-\beta}{1+\beta}\right)\right),$$

$$J_v = \underset{\sim}{J}_v \Big/ \left(1 + e\left(\frac{1-\beta}{1+\beta}\right)\right); \tag{2-36}$$

with a similar set of expressions for M_u and M_v.

The solution for the normal components is more direct as (2-15) and (2-18) can be written as

$$\underset{\sim}{H}_n \left(1 + \frac{\underset{\sim}{\beta}}{\mu_r}\right) = 2\, H_n^i + \hat{n} \cdot \left(\vec{I} - \underset{\sim}{\beta}\, \vec{I}_1\right) ,$$

$$\underset{\sim}{E}_n \left(1 + \frac{\underset{\sim}{\alpha}}{\varepsilon_r}\right) = 2\, E_n^i + \hat{n} \cdot \left(\vec{K} - \underset{\sim}{\alpha}\, \vec{K}_1\right) . \qquad (2\text{-}37)$$

Here

$$H_n = \underset{\sim}{H}_n \Big/ \left(1 + e_s \frac{\left(1 - \underset{\sim}{\beta}/\mu_r\right)}{\left(1 + \underset{\sim}{\beta}/\mu_r\right)}\right)$$

and

$$E_n = \underset{\sim}{E}_n \Big/ \left(1 + e_s \frac{\left(1 - \underset{\sim}{\alpha}/\varepsilon_r\right)}{\left(1 + \underset{\sim}{\alpha}\, \varepsilon_r\right)}\right)$$

where e_s is defined in equation (2-23).

Note some interesting things about the solution (2-34). Suppose we have $\underset{\sim}{\beta} = 1/\varepsilon_r$ and $\underset{\sim}{\alpha} = 1/\mu_r$, then the cross terms disappear. This is convenient, because the terms which have γ in them are the result of the self-patch calculation. They are large and inherently inaccurate. (The self-patch term involving e is small.) The equations thus reduce to

$$\left(1 + \frac{1}{\varepsilon_r}\right) \underset{\sim}{\vec{J}} = 2\, \vec{J}^i + \hat{n} \times \left(\vec{I} - \frac{1}{\varepsilon_r}\, \vec{I}_1\right)$$

$$\left(1 + \frac{1}{\mu_r}\right) \underset{\sim}{\vec{M}} = 2\, M^i - \hat{n} \times \left(\vec{K} - \frac{1}{\mu_r}\, \vec{K}_1\right) \qquad (2\text{-}38)$$

That is, by choice of the weighting factors $\underset{\sim}{\alpha}$ and $\underset{\sim}{\beta}$, we were able to eliminate the annoying large self-patch contribution. We might expect this choice of $\underset{\sim}{\alpha}$ and $\underset{\sim}{\beta}$ to give the best results. In practice it was found that results for the sphere were most accurate and stable for $\underset{\sim}{\alpha} = 1/\mu_r = 1$, but $\underset{\sim}{\beta} \approx .7\ 1/\varepsilon_r$.

We also note that the limit $\varepsilon_r \to \infty$, $\mu_r \to 0$ such that $\varepsilon_r \mu_r$ remains finite represents the conductor. In fact, equations (2-34) do reduce to the single equation used in [5,6] and Section 3 for the conducting case:

$$\underset{\sim}{\vec{J}} = 2 \vec{J}^i + \hat{n} \times \vec{I} \ . \qquad (2\text{-}39)$$

2.3 RESULTS OF THE STIE CALCULATION

The integral equation solution was tested for the shapes illustrated in Figure 2-2, namely the sphere and sphere-capped cylinder, both with $\varepsilon_r = 3$. For the sphere, computational results could be compared directly with the results from the classical solution. This comparison is given in Figure 2-3. The incident pulse was the smoothed impulse of equation (2-20) with $a_n = 0.5$. As can be seen, the agreement is nearly exact. It is interesting to compare the response with that of a conducting sphere, shown in Figure (2-2b) with a vertical scale reduced by a factor of 2.

The computed response of the sphere-capped cylinder is shown in Figures 2-4 and 2-5 for TE and TM polarizations and at various angles of incidence. The second bump in these responses is interpreted as the result of an internally propagated wave, which is partially reflected at the backside and reradiated upon re-emergence from the front.

In Figures 2-6 and 2-7 are shown the results of comparing these calculated responses with those measured on the scattering range (Section 4). The measured responses were here transformed by a convolution procedure to obtain the response to the standard incident pulse, thus permitting direct comparison.

The parameters of the sphere were: 8 bands of approximately equal sized patches, with a total of 40 patches on the hemisphere (plane symmetry was utilized requiring the computation of the hemisphere only); radius = 1; $\varepsilon_r = 3.0$, $\mu_r = 1.0$. The time step of the solution was $\Delta t = .333$, while the solution parameters $\underset{\sim}{\beta}$, $\underset{\sim}{\alpha}$ were .22 and 1.0. The actual values of $\underset{\sim}{\beta}$ and $\underset{\sim}{\alpha}$ had only a weak effect on the solution.

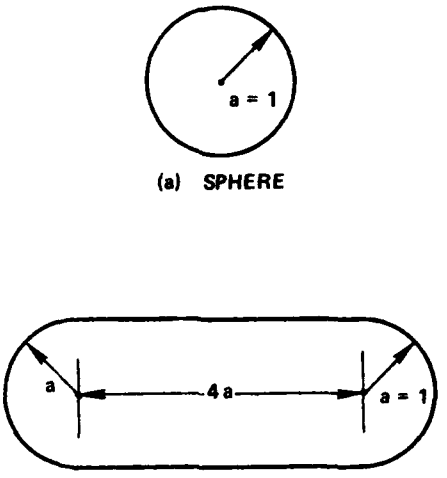

FIG. 2-2 Test targets for STIE solution.

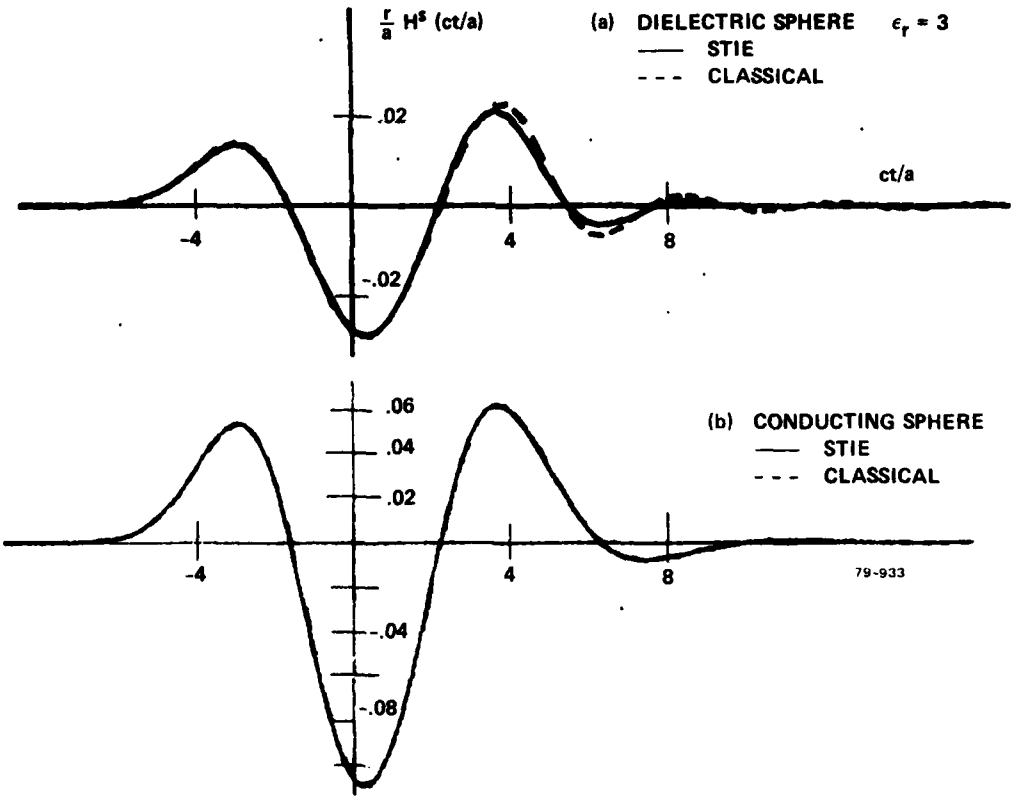

FIG. 2-3 Smoothed impulse response — sphere: $a_n = 1/2$, $\epsilon_r = 3$ (STIE).

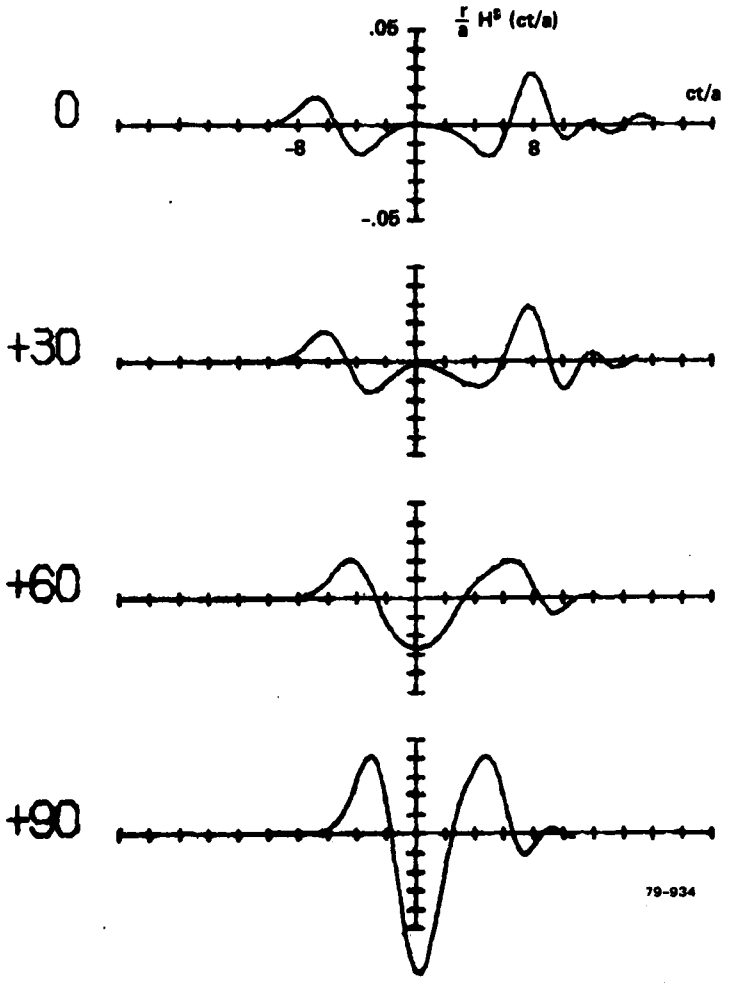

FIG. 2-4 Smoothed impulse response – sphere capped cylinder: $a_n = 1/2$, $\epsilon_r = 3$, TE (STIE).

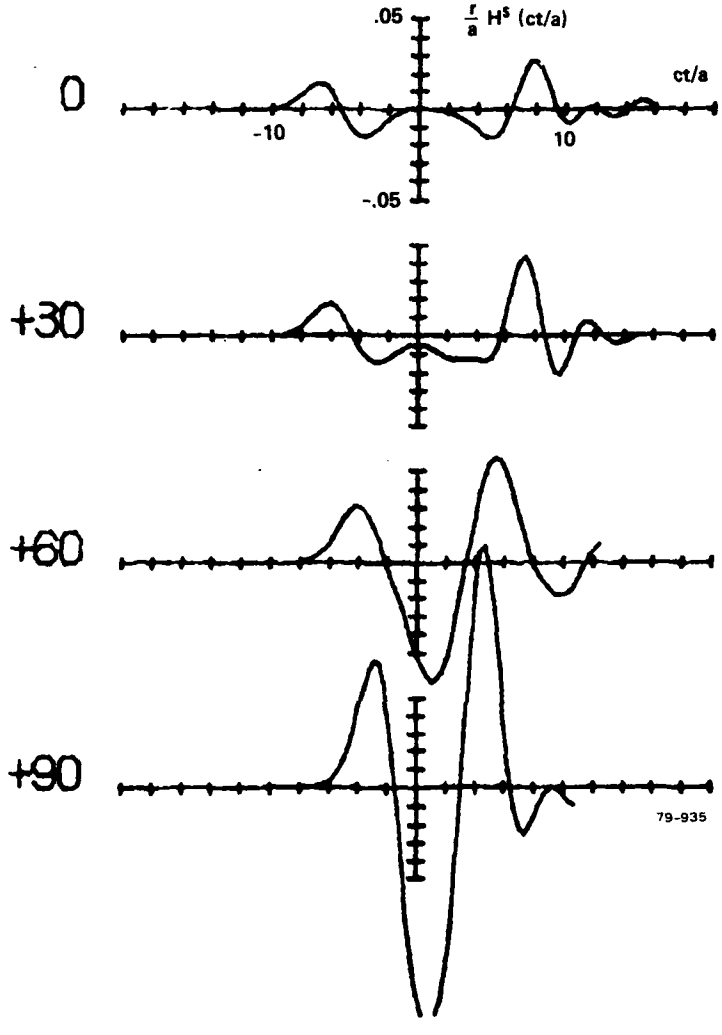

FIG. 2-5 Smoothed impulse response — sphere capped cylinder: $a_n = 1/2$, $\epsilon_r = 3$, TM (STIE).

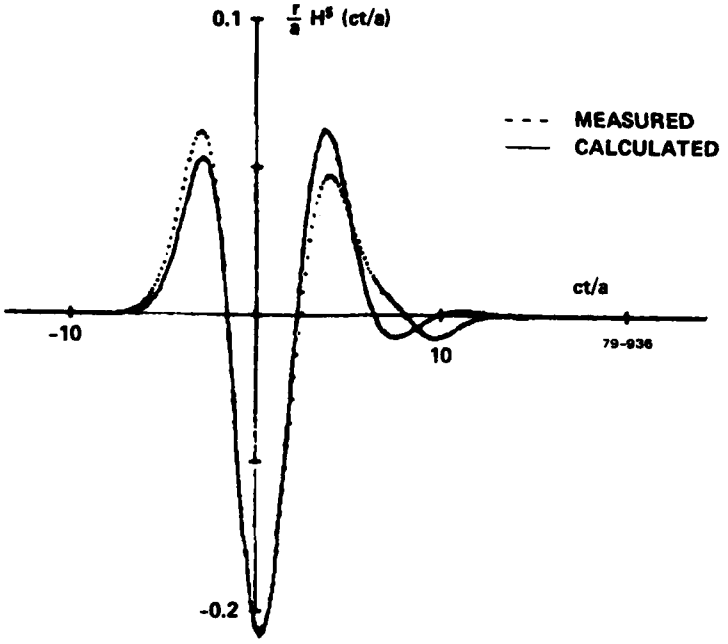

FIG. 2-6 Comparison of measured and calculated responses — conducting sphere.

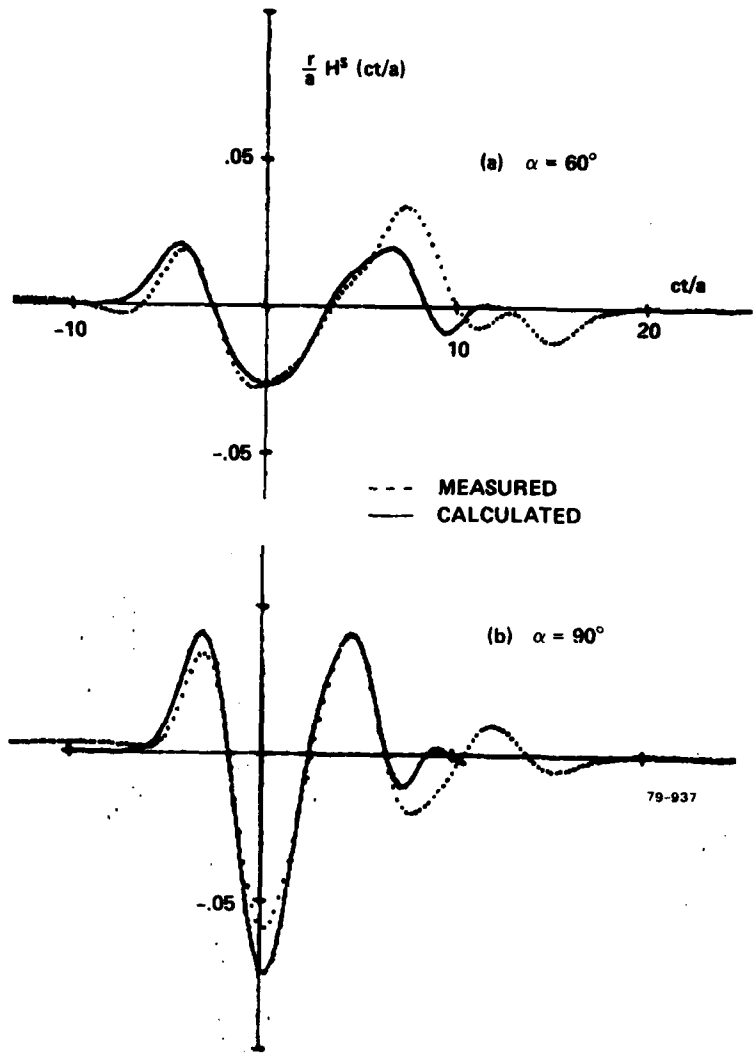

FIG. 2-7 Comparison of measured and calculated responses — dielectric sphere capped cylinder ($\epsilon_r = 3$).

The sphere capped cylinder parameters were the same, except for the insertion of 8 bands of 8 patches each representing the cylinder body.

2.4 CLASSICAL SOLUTION FOR DIELECTRIC SPHERES

The eigenfunction solution for the sphere is given by Stratton [1] among others. The method consists of expanding the incident plane wave, the scattered wave, and the interior wave in terms of spherical wave functions. The latter form a complete set of independent solutions to the wave equation. The boundary conditions are then applied and the coefficients of like functions equated. We collect here the pertinent equations. The geometry is still that of Figure (2-1), except that the target is a sphere.

The incident plane wave from the positive z direction can be written

$$\vec{E}^i = \hat{x}\, E_o\, e^{-ikz - i\omega t} \equiv E_o\, e^{-i\omega t} \sum_{n=1}^{\infty} (-i)^n \frac{(2n+1)}{n(n+1)} \left(\vec{m}^{(1)}_{oln} + i\, \vec{n}^{(1)}_{eln} \right) \tag{2-40}$$

$$\vec{H}^i = -\hat{y} \sqrt{\frac{\varepsilon}{\mu}}\, E_o\, e^{-ikz - i\omega t} = \sqrt{\frac{\varepsilon}{\mu}}\, E_o e^{-i\omega t} \sum_{n=1}^{\infty} \frac{(2n+1)}{n(n+1)} \left(\vec{m}^{(1)}_{eln} - i\, \vec{n}^{(1)}_{oln} \right) \tag{2-41}$$

The spherical wave functions are

$$\vec{m}^{(1)}_{\substack{oln \\ e}} = \pm \frac{1}{\sin\theta}\, j_n(kr)\, P^1_n(\cos\theta) \begin{matrix} \cos\phi \\ \sin\phi \end{matrix} \hat{\theta} - j_n(kr) \frac{\partial P^1_n}{\partial \theta} \begin{matrix} \sin\phi \\ \cos\phi \end{matrix} \hat{\phi} \tag{2-42}$$

$$\vec{n}^{(1)}_{\substack{oln \\ e}} = \frac{n(n+1)}{kr}\, j_n(kr)\, P^1_n(\cos\theta) \begin{matrix} \sin\phi \\ \cos\phi \end{matrix} \hat{r} + \frac{1}{kr} \left[kr\, j_n(kr) \right]' \frac{\partial P^1_n}{\partial \theta} \begin{matrix} \sin\phi \\ \cos\phi \end{matrix} \hat{\theta}$$

$$\pm \frac{1}{kr \sin\theta} \left[kr\, j_n(kr) \right]' P^1_n(\cos\theta) \begin{matrix} \cos\phi \\ \sin\phi \end{matrix} \hat{\phi} \tag{2-43}$$

In the preceding rather complicated expression, the subscript o means odd, e means even. On the right-hand side the upper of sin ϕ or cos ϕ refers to the odd form, the lower to the even form; similarly the lower of the $\pm$ sign refers to the even form. The quantity $[...]'$ means $\partial/\partial(kr)\ [...]$. The wave number $k = \omega/c = \omega\sqrt{\varepsilon\mu}$.

The superscript (1) refers to the appearance of the first kind spherical Bessel function, $j_n(kr)$. The first kind Bessel function is finite at the origin and is therefore used in the incident wave as well as the interior wave. The third kind spherical Bessel function $h_n^{(1)}(kr)$ appears in the scattered wave expression, since it is outward traveling and finite at infinity; its appearance in the wave function will be indicated as $\vec{m}_{oln}^{(3)}$, etc. The function P_n^1 (cos θ) is the Associated Legendre polynomial. It is given by

$$P_n^1 (\cos\theta) = \sin\theta \frac{d P_n (\cos\theta)}{d (\cos\theta)} ,$$

where the Legendre polynomial is found recursively by

$$n P_n(x) = x (2n-1) P_{n-1}(x) - (n-1) P_{n-2}(x) \qquad (2\text{-}45)$$

the scattered field is written

$$\vec{E}^s = E_o e^{-i\omega t} \sum_{n=1}^{\infty} (-i)^n \frac{(2n+1)}{n(n+1)} \left(a_n^s \vec{m}_{oln}^{(3)} + i b_n^s \vec{n}_{eln}^{(3)} \right) \qquad (2\text{-}46)$$

$$\vec{H}^s = \sqrt{\frac{\varepsilon}{\mu}}\ E_o e^{-i\omega t} \sum_{n=1}^{\infty} (-i)^n \frac{(2n+1)}{n(n+1)} \left(b_n^s \vec{m}_{eln}^{(3)} - i a_n^s \vec{n}_{oln}^{(3)} \right) \qquad (2\text{-}47)$$

In the interior, we have similar expressions for $\vec{E}^t$ and $\vec{H}^t$ (transmitted wave), except that ε, μ, c, k are replaced by ε_1, μ_1, c_1, k_1; the coefficients are a_n^t and b_n^t and the eigenfunctions contain spherical Bessel functions of the first kind. We now evaluate these equations at the boundary r = a and apply the boundary conditions, namely

$$\hat{r} \times \left(\vec{E}^i + \vec{E}^s\right) = \hat{r} \times \vec{E}^t \ ,$$

$$\hat{r} \times \left(\vec{H}^i + \vec{H}^s\right) = \hat{r} \times \vec{H}^t \qquad (2\text{-}48)$$

(The boundary conditions on the normal components are not required.) The result is a set of 4 equations in the four unknowns a_n^s, b_n^s, a_n^t, b_n^t, for each n:

$$\begin{bmatrix} -h_n^{(1)}(x) & j_n(x_1) \\ -\dfrac{\left[x\, h_n^{(1)}(x)\right]'}{\mu} & \dfrac{\left[x_1\, j_n(x_1)\right]'}{\mu_1} \end{bmatrix} \begin{bmatrix} a_n^s \\ a_n^t \end{bmatrix} = \begin{bmatrix} j_n(x) \\ \dfrac{\left[x\, j_n(x)\right]'}{\mu} \end{bmatrix} \qquad (2\text{-}49)$$

$$\begin{bmatrix} -\sqrt{\dfrac{\varepsilon}{\mu}}\, h_n^{(1)}(x) & \sqrt{\dfrac{\varepsilon_1}{\mu_1}}\, j_n(x_1) \\ -\dfrac{\left[x\, h_n^{(1)}(x)\right]'}{\sqrt{\varepsilon\mu}} & \dfrac{\left[x_1\, j_n(x_1)\right]'}{\sqrt{\varepsilon_1\mu_1}} \end{bmatrix} \begin{bmatrix} b_n^s \\ b_n^t \end{bmatrix} = \begin{bmatrix} \sqrt{\dfrac{\varepsilon}{\mu}}\, j_n(x) \\ \dfrac{\left[x\, j_n(x)\right]'}{\sqrt{\varepsilon\mu}} \end{bmatrix} \qquad (2\text{-}50)$$

where $x = ka$, $x_1 = k_1 a$, $k_1 = \omega/c_1$.

The above are solved directly for a_n^s and b_n^s, the coefficients of the scattered field. For the far scattered field we use the asymptotic form as $r \to \infty$. For instance, at $\phi = 0$

$$\vec{m}_{eln}^{(3)} = -h_n^{(1)}(kr)\, \frac{dP_n^1}{d\theta}\, \hat{\phi} \to i\, \frac{e^{ikr}}{kr}\, (-i)^n\, \frac{dP_n^1}{d\theta}\, \hat{\phi}$$

$$i\, \vec{n}_{oln}^{(3)} = i\, \frac{\left[kr\, h_n^{(1)}(kr)\right]'}{kr}\, \frac{P_n^1}{\sin\theta}\, \hat{\phi} \to i\, \frac{e^{ikr}}{kr}\, (-i)^n\, \frac{P_n^1}{\sin\theta}\, \hat{\phi}$$

For the other polarization, we use $\phi = 90^\circ$; then

$$\vec{m}^{(3)}_{eln} = -h_n^{(1)}(kr)\,\frac{P_n^1}{\sin\theta}\,\hat{\theta} \to i\,\frac{e^{ikr}}{kr}\,(-i)^n\,\frac{P_n^1}{\sin\theta}\,\hat{\theta}$$

$$i\,\vec{n}^{(3)}_{oln} = i\,\frac{\left[kr\,h_n^{(1)}\,kr\right]'}{kr}\,\frac{dP_n^1}{d\theta}\,\hat{\theta} \to i\,\frac{e^{ikr}}{kr}\,(-i)^n\,\frac{dP_n^1}{d\theta}\,\hat{\theta}$$

Hence, the (normalized) result in the $\phi = 0$ plane (E-plane)

$$\left(-\frac{rH^s}{a}\right) = i\,\frac{(-1)^n}{ka}\,\frac{(2n+1)}{n(n+1)}\left[\frac{P_n^1}{\sin\theta}\,a_n^s - \frac{dP_n^1}{d\theta}\,b_n^s\right]\hat{y}\ ; \qquad (2\text{-}51)$$

$$\left(-\frac{rH^s}{a}\right) = i\,\frac{(-1)^n}{ka}\,\frac{(2n+1)}{n(n+1)}\left[\frac{dP_n^1}{d\theta}\,a_n^s - \frac{P_n^1}{\sin\theta}\,b_n^s\right]\hat{\theta}\ . \qquad (2\text{-}52)$$

In the backscatter direction $\theta = 0^\circ$, we have

$$\frac{P_n^1}{\sin\theta} = \frac{dP_n^1}{d\theta} = \frac{n(n+1)}{2}\ ,$$

so that the term in brackets becomes $[a_n^s - b_n^s]$.

2.5 SOLUTION FOR TARGETS WITH DISPERSIVE CONSTITUTIVE PARAMETERS

In the above consideration, the constitutive parameters of the scattering body (μ_1, ε_1) were taken to be independent of frequency. That is, the impulse response of the material is an impulse. For many dielectric materials that might be used for target construction this assumption is valid over the range of operating frequencies that may be encountered in practice. However, there also exist materials and situations where this assumption of frequency independence is not valid.

2.5.1 Radar Absorbing Materials on Conducting Surfaces

Radar Absorbing Materials (RAM), for example, typically possess constitutive parameters which are strongly dependent upon the frequency of the

illuminating waveform. In this case the RAM is attached to the skin of a conducting target and its effect may be accounted for by use of a surface impedance which couples the tangential $\vec{E}$ and $\vec{H}$ field on the surface by:

$$\hat{n} \times \vec{E} = Z_c * \left[(\hat{n} \times \vec{H}) \times \hat{n} \right] \tag{2-53}$$

where

Z_c = the impulse response of the RAM surface impedance

$*$ = the convolution operation

Note that in this case there again is no penetration of the fields inside the target by virtue of the fact that it has a conducting skin. These two features reduce the problem to the solution of one integral equation that is derivable from (2-1) by use of the impedance boundary condition (2-53) and the boundary condition that $\hat{n} \cdot \vec{H} = 0$. This space-time integral equation is given by:

$$\hat{n} \times \vec{H}(\vec{r},t) = 2\hat{n} \times \vec{H}^i(\vec{r},t) + \frac{1}{2\pi} \int \hat{n} \times \left\{ L(\hat{n}' \times \vec{H}) \times \hat{R} + \frac{1}{R} \left[\hat{n}' \times \left(Z_c * \frac{\partial \vec{H}}{\partial \tau} \right) \right] \times \hat{n}' \right\}_{\tau = t - R} dS' \tag{2-54}$$

where

$$Z_c * \vec{H} = \int_{-\infty}^{t} \vec{H}(\tau)\, Z_c(\tau - t)\, d\tau$$

The solution of the space-time integral equation in (2-54) is carried out in the same manner as has been used for the case of perfectly conducting targets. The problem is solved numerically for the tangential surface field $\hat{n} \times \vec{H}$ by marching the solution on in time. In this case, however, a second term appears within the integral on the right-hand side of (2-54). It is this term that will tend to reduce the tangential field setup, and thus, the scattered return. The value of this term results from the convolution of the $\vec{H}$ field with the impulse response of the RAM. This

convolution can be computed numerically in the time domain since it uses only previously computed values of $\vec{H}$.

2.5.2 Lossy Materials

Lossy materials may be modeled by allowing an electric current to flow within the material. In this model Maxwell's equations are written:

$$\nabla \times \vec{H} = \frac{\partial \vec{D}}{\partial t} + \vec{J}$$

$$\nabla \times \vec{E} = - \frac{\partial \vec{B}}{\partial t} \qquad (2\text{-}55)$$

For the case where linearity exists, then the constitutive relations are

$$\vec{D} = \varepsilon * \vec{E}$$

$$\vec{B} = \mu * \vec{H}$$

$$\vec{J} = \sigma * \vec{E} \qquad (2\text{-}56)$$

where ε, μ, and σ represent the impulse response of the constitutive parameters. If these impulse responses are impulses, then the convolution becomes a simple product. Moreover, the problem is still dispersive. Equation (2-55) becomes

$$\nabla \times \vec{H} = \varepsilon \frac{\partial \vec{E}}{\partial t} + \sigma \vec{E}$$

$$\nabla \times \vec{E} = - \mu \frac{\partial \vec{H}}{\partial t} \qquad (2\text{-}57)$$

The Fourier transform of these equations give their frequency domain counter part as

$$\nabla \times \vec{H} = (j\omega \varepsilon + \sigma) \vec{E}$$

$$\nabla \times \vec{E} = - j\omega \mu \vec{H} \qquad (2\text{-}58)$$

where

$$H(\vec{r},t) \leftrightarrow H(\vec{r},\omega)$$

$$E(\vec{r},t) \leftrightarrow E(\vec{r},\omega)$$

and an equivalent permittivity $\underset{\sim}{\varepsilon}$ may be written

$$\underset{\sim}{\varepsilon} = \varepsilon\left(1 + \frac{\sigma}{j\omega\varepsilon}\right) \tag{2-59}$$

The time domain solution of this problem may be carried out in several ways.

One approach would be to solve the frequency domain integral equation for the complex ε at the frequencies contained within the spectrum of the incident waveform and do the inverse transform of the weighted result. This approach is both computer time and memory intensive.

A second approach would be to solve Maxwell's equations (2-57) directly in the time domain throughout the volume of space that encloses the target and its neighborhood using an extension of the technique first proposed by Yee [9] and subsequently by Taflove [10]. This approach is computer memory intensive and yields only approximate results, since workers to date have been unable to account exactly for the effect of the solution volume boundary on the numerical results.

A Third approach would be to develop and solve the space-time integral equation. The frequency domain integral equations for the fields inside the body are

$$\vec{H}_1(\vec{r},\omega) = -\frac{1}{4\pi}\int_S \left\{\left[\frac{1}{R}\left(j\omega\underset{\sim}{\varepsilon}_1\right)\hat{n}' \times \vec{E}_1\right] + \left[\frac{1}{R^2} + \frac{1}{R}(j\omega/c)\right]\left[\hat{n}' \cdot \vec{H}_1 + \left(\hat{n}' \times \vec{H}_1\right) \times \hat{R}\right]\right\} e^{-j\omega R/c}\, dS' \tag{2-60}$$

$$\vec{E}_1(\vec{r},\omega) = -\frac{1}{4\pi}\int_S \left\{\left[\frac{1}{R}\left(-j\omega\mu_1\right)\hat{n}' \times \vec{H}_1\right]\right.$$

$$\left. + \left[\frac{1}{R^2} + \frac{1}{R}\left(j\omega/c\right)\right]\left[\left(\hat{n}' \cdot \vec{E}_1\right) + \left(\hat{n}' \times \vec{E}_1\right) \times \hat{R}\right]\right\} e^{-j\omega R/c}\, dS' \qquad (2\text{-}61)$$

In this case

$$\frac{1}{c} = \sqrt{\mu_1\varepsilon_1}\left(1 + \frac{\sigma}{j\omega\varepsilon_1}\right)^{\frac{1}{2}} \qquad (2\text{-}62)$$

Consider the case where losses are low so that

$$\frac{\sigma}{\omega\varepsilon_1} << 1$$

and then (2-62) becomes

$$\frac{1}{c} = \frac{1}{c_1}\left(1 + \frac{\sigma}{j\omega 2\varepsilon_1}\right) \qquad (2\text{-}63)$$

where

$$\frac{1}{c_1} = \sqrt{\mu_1\varepsilon_1}$$

Substitution of (2-63) in (2-60) and (2-61) yields

$$\vec{H}_1(\vec{r},\omega) = -\frac{1}{4\pi}\int_S \left\{\left[\frac{1}{R}\left(j\omega\varepsilon_1 + \sigma\right)\hat{n}' \times \vec{E}_1\right]\right.$$

$$\left. + \left[\frac{1}{R^2} + \frac{1}{R}\frac{\sigma}{2}\sqrt{\frac{\mu_1}{\varepsilon_1}} + \frac{1}{R}\frac{j\omega}{c_1}\right]\left[\left(\hat{n}' \cdot \vec{H}_1\right) + \left(\hat{n}' \times \vec{H}_1\right) \times \hat{R}\right]\right\}$$

$$e^{-j\omega R/c_1}\, e^{-R\left(\frac{\sigma}{2}\sqrt{\frac{\mu_1}{\varepsilon_1}}\right)}\, dS' \qquad (2\text{-}64)$$

$$\vec{E}_1(\vec{r},\omega) = -\frac{1}{4\pi}\int_S \left\{\left[\frac{1}{R}\left(-j\omega\mu_1\right)\hat{n}' \times \vec{H}_1\right]\right.$$

$$\left. + \left[\frac{1}{R^2} + \frac{1}{R}\left(\frac{\sigma}{2}\sqrt{\frac{\mu_1}{\varepsilon_1}}\right) + \frac{1}{R}\frac{j\omega}{c_1}\right]\left[\left(\hat{n}' \cdot \vec{H}_1\right) + \left(\hat{n}' \times \vec{H}_1\right) \times R\right]\right\}$$

$$e^{-j\omega R/c_1}\ e^{-R\left(\frac{\sigma}{2}\sqrt{\frac{\mu_1}{\varepsilon_1}}\right)}\ dS' \qquad (2\text{-}65)$$

The space-time integral equations are now obtained by taking the Fourier transform of (2-64) and (2-65). The result is

$$\vec{H}_1(\vec{r},t) = -\frac{1}{4\pi}\int_S \left\{\left[\frac{1}{R}\left(\sigma + \sqrt{\frac{\varepsilon_1}{\mu_1}}\ \frac{1}{c_1}\ \frac{\partial}{\partial\tau}\right)\left(\hat{n}' \times \vec{E}_1''\right)\right]\right.$$

$$\left. + \mathcal{L}_1\left[\left(\hat{n}' \cdot \vec{H}_1''\right) + \left(\hat{n}' \times \vec{H}_1''\right) \times \hat{R}\right]\right\} e^{-\alpha R}\ dS' \qquad (2\text{-}66)$$

$$\tau = t - R/c_1$$

$$\vec{E}_1(\vec{r},t) = -\frac{1}{4\pi}\int_S \left\{\left[-\frac{1}{R}\sqrt{\frac{\mu_1}{\varepsilon_1}}\ \frac{1}{c_1}\ \frac{\partial}{\partial\tau}\left(\hat{n}' \times \vec{H}_1''\right)\right]\right.$$

$$\left. + \mathcal{L}_1\left[\left(\hat{n}' \cdot \vec{E}_1''\right) + \left(\hat{n}' \times \vec{E}_1''\right) \times \hat{R}\right]\right\} e^{-\alpha R}\ dS' \qquad (2\text{-}67)$$

where

$$\mathcal{L}_1 = \left(\frac{1}{R^2} + \frac{1}{R}\left(\frac{\sigma}{2}\sqrt{\frac{\mu_1}{\varepsilon_1}}\right) + \frac{1}{Rc_1}\ \frac{\partial}{\partial\tau}\right)$$

$$\alpha = \frac{\sigma}{2}\sqrt{\frac{\mu_1}{\varepsilon_1}}$$

These space-time integral equations correspond to those given in (2-3) and (2-4) for the lossless target case. The solution is carried out numerically in the same manner as was described earlier by stepping on in time. It is interesting to note that the effect of losses is to add an attenuation factor $e^{-\alpha R}$ to the integrand of (2-66) and (2-67). There also appears an attenuation term in the $\hat{L}_1$ operator which is proportional to the conductivity σ. This solution will be valid for the case where

$$\varepsilon \frac{\partial \vec{E}_1}{\partial t} >> \sigma \vec{E}_1 \tag{2-68}$$

when this is not valid then the direct solution of Maxwell's equations in the time domain appears to be the best approach.

2.5.3 Dispersive Dielectric Materials

In this section the case of dielectric materials whose permittivity varies with frequency is considered. That is

$$\varepsilon = \varepsilon(\omega)$$

so that in the time domain

$$\vec{D} = \varepsilon * \vec{E}$$

For simplicity the magnetic properties are constant and the conductivity is zero:

$$\mu = \text{constant}$$
$$\sigma = 0$$

For this case Maxwell's equations become

$$\nabla \times \vec{H} = \varepsilon * \frac{\partial \vec{E}}{\partial t}$$

$$\nabla \times E = - \mu \frac{\partial \vec{H}}{\partial t} \tag{2-69}$$

where

$$\varepsilon * \vec{E} = \int_{-\infty}^{t} \vec{E}(\tau)\, \varepsilon(\tau - t)\, d\tau \quad . \tag{2-70}$$

One approach is to solve (2-69) numerically using (2-70) in a volume of space that includes the target and its neighborhood by marching on in time. A second approach is to solve the frequency domain integral equations for the dispersive permittivity and to inverse transform the weighted result. The development of a space-time integral equation can be reduced to the development of a Greens function in the time domain for a dispersive medium. To do this a physical model for the dispersion would be helpful and perhaps necessary. To date a space-time integral equation for general dispersive media has not been developed. The problem solution could be carried out by solving Maxwell's equations directly or by solving the frequency domain integral equation and inverse transforming the result.

SECTION III

SPACE-TIME INTEGRAL EQUATION SOLUTION - COMPLEX CONDUCTING TARGET

The space-time integral equation formulation is valid for any target shape. Solution techniques have been developed for a number of important shapes for the case of conducting targets [5][6]. In particular, flat plates and cylinders have been treated. These shapes have also been combined to form the solution to scattering from an aircraft or missile model. In this section the solution for a Tomahawk Cruise missile model is given. The model is a long thin sphere-capped cylinder with flat rectangular plates for wings and stabilizers. This shape very closely resembles the missile. The theory of the solution is reviewed in Subsections 3.1 and 3.2; followed by the computed results and comparison with measurement.

3.1 THEORY OF THE SPACE-TIME INTEGRAL EQUATION SOLUTION FOR SCATTERING FROM A CONDUCTING MISSILE MODEL

The problem of determining the scattering by cylinders with fins attached is of great practical interest, since this serves as a model for numerous missiles and aircraft. Basically this approach consists of developing two simultaneous space-time integrodifferential equations and their subsequent computer solution by marching on in time. These equations contain terms which may be interpreted as:

(a) The influence of cylinder currents on other cylinder currents.

(b) The influence of fin currents on cylinder currents.

(c) The influence of fin currents on other fin currents.

(d) The influence of cylinder currents on fin currents.

The neighborhood along the line where a fin is attached to the cylinder is accounted for by application of boundary conditions at the edge of the fin.

The boundary condition for a conductor is that $\hat{n} \times \vec{E} = 0$. In addition it is true that $H_n = 0$ on the surface. The equation for the total field in terms of its surface values then becomes (compare (2-1))

$$\vec{H}(\vec{r},t) = \vec{H}^i(\vec{r},t) + \frac{1}{4\pi}\oint_s L(\hat{n}'\times\vec{H}')\times\hat{R}\,dS' \qquad (3\text{-}1)$$

where

$$\vec{H}' = \vec{H}(\vec{r}',\tau)$$

$$L = \frac{1}{R^2} + \frac{1}{Rc}\frac{\partial}{\partial\tau}$$

$$\vec{R} = \vec{r} - \vec{r}'$$

$$\tau = t - R/c$$

We will normalize time to light-meters (c = 1). On the surface of a conductor, (2-11) simplifies to

$$\vec{J}(\vec{r},t) = 2\vec{J}^i(\vec{r},t) + \frac{1}{2\pi}\oint_s \hat{n}\times\left\{L\vec{J}'\times\hat{R}\;dS'\right\} \qquad (3\text{-}2)$$

The above is the result of applying a limiting process to (3-1) in moving the observation point $\vec{r}$ to S. We proceed as in Section 2. An incident field is applied of form

$$|H^i| = \frac{a_n}{\sqrt{\pi}}\;e^{-\left(a_n t\right)^2} \qquad (3\text{-}3)$$

and (3-2) is first solved numerically for all time by a marching-in-time procedure. Having found the surface currents, the farscattered field is obtained by application of the asymptotic form of (3-1)

$$r\vec{H}^s\left(\vec{r},t_f\right) = \frac{1}{4\pi}\oint_s \frac{\partial\vec{J}(\vec{r}',t')}{\partial t}\times\hat{r}\,dS' \qquad (3\text{-}4)$$

$$t' = t_f + \vec{r}'\cdot\hat{r}_o\ .$$

Equation (3-2) for $\vec{J}$ on S is applied on the surface of a conducting solid. For the thin conducting surface a different formulation is used.

The integrodifferential equation for the fin currents is obtained by starting with the expression for the electric and magnetic potentials. The total electric field is given by

$$\vec{E}(\vec{r},t) = \vec{E}^{i}(\vec{r},t) - \mu \frac{\partial \vec{A}(\vec{r},t)}{\partial t} - \nabla\phi(\vec{r},t) \qquad (3\text{-}5)$$

where

$\vec{A}$ = magnetic vector potential such that $\vec{H} = \nabla \times \vec{A}$

ϕ = electric potential

μ = permeability of space.

Next, apply to (3-5) the Lorentz gauge relation

$$\nabla \cdot \vec{A} + \varepsilon \frac{\partial \phi}{\partial t} = 0$$

where ε is the permittivity of space, yielding

$$\varepsilon \frac{\partial \vec{E}(\vec{r},t)}{\partial t} = \varepsilon \frac{\partial \vec{E}^{i}(\vec{r},t)}{\partial t} + \nabla(\nabla \cdot \vec{A}) - \mu\varepsilon \frac{\partial^2 \vec{A}(\vec{r},t)}{\partial t^2} . \qquad (3\text{-}6)$$

Then applying the E-field boundary condition that the component of the total E-field tangent to the fin vanishes everywhere on the fin, (3-6) can be expressed as

$$\nabla\left(\nabla \cdot \vec{A}(\vec{r},t)\right) - \frac{\partial^2 \vec{A}(\vec{r},t)}{\partial t^2} = -\varepsilon \frac{\partial \vec{E}^{i}(\vec{r},t)}{\partial t} \qquad (3\text{-}7)$$

or, in a more simplified form

$$\square^2 \vec{A} + \boxtimes \vec{A} = -\varepsilon \frac{\partial \vec{E}^{i}}{\partial t} \qquad (3\text{-}8)$$

where

$$\Box^2\vec{A} = \left(\frac{\partial^2}{\partial x^2} - \frac{\partial^2}{\partial t^2}\right) A_x\hat{a}_x + \left(\frac{\partial^2}{\partial y^2} - \frac{\partial^2}{\partial t^2}\right) A_y\hat{a}_y + \left(\frac{\partial^2}{\partial z^2} - \frac{\partial^2}{\partial t^2}\right) A_z\hat{a}_z ,$$

the wave operator.

$$\boxed{x}\vec{A} = \frac{\partial}{\partial x}\left(\frac{\partial A_y}{\partial y} + \frac{\partial A_z}{\partial z}\right)\hat{a}_x + \frac{\partial}{\partial y}\left(\frac{\partial A_z}{\partial z} + \frac{\partial A_x}{\partial x}\right)\hat{a}_y + \frac{\partial}{\partial z}\left(\frac{\partial A_x}{\partial x} + \frac{\partial A_y}{\partial y}\right)\hat{a}_z$$

$$\vec{A}(\vec{r},t) = \frac{1}{4\pi}\int\left\{\frac{J(\vec{r}',\tau)}{R}\right\} dS' .$$

$$\tau = t - R$$

To form the above expansion, the fins are assumed to lie in the x - z plane. In order to obtain an expression for the fin currents directly, it is necessary to express the magnetic vector potential $\vec{A}$ as the sum of two components, one due to the observation point ("self" patch) and the other due to the remainder of the patches. If the fin grid patches are small enough, then the current over a given patch can be assumed constant. This makes it possible to express $\vec{A}$ as

$$\vec{A}(\vec{r},t) = \gamma_F\vec{J}_F(\vec{r},t) + \frac{1}{4\pi}\int_{\substack{\text{Non-self}\\ \text{Patches}}}\left\{\frac{\vec{J}(\vec{r}',\tau)}{R}\right\} dS' \quad \tau = t - R . \qquad (3\text{-}9)$$

where

$$\gamma_F = \left(\sqrt{\frac{\Delta S}{\pi} - \left(\frac{\delta}{2}\right)^2} - \frac{\delta}{2}\right)\Big/ 2 .$$

ΔS = area of patch containing $\vec{r}$

δ = thickness of fin

Substituting this into (3-8) yields the fin currents directly as

$$\nabla^2 \vec{J}_F(\vec{r},t) + \underline{x}\, \vec{J}_F(\vec{r},t) = \frac{1}{\gamma} \left\{ - \varepsilon \frac{\partial E^i}{\partial t} - \nabla^2 \vec{A}_{NS}(\vec{r},t) - \underline{x}\, \vec{A}_{NS}(\vec{r},t) \right\} \quad (3\text{-}10)$$

where

$$\vec{A}_{NS} = \frac{1}{4\pi} \int_{\substack{\text{Non-Self} \\ \text{Patches}}} \left\{ \frac{\vec{J}(\vec{r}',\tau)}{R} \right\} dS' \qquad \tau = t - R$$

The surface currents contributing to A_{NS} are both cylinder currents and fin currents. The contribution of both of these can be separated in (3-10) and displayed explicitly to give the expression for the current flowing on the fin

$$\nabla^2 \vec{J}_F(\vec{r},t) + \underline{\underline{x}}\, \vec{J}_F(\vec{r},t) = \frac{1}{\gamma_F} \left\{ -\varepsilon \frac{\partial E^i}{\partial t} - \nabla^2 \left[\vec{A}_{F_{NS}}(\vec{r},t) + \vec{A}_C(\vec{r},t) \right] \right.$$

$$\left. - \underline{\underline{x}} \left[\vec{A}_{F_{NS}}(\vec{r},t) + \vec{A}_C(\vec{r},t) \right] \right\} \quad (3\text{-}11)$$

where $\vec{A}_C(\vec{r},t)$ is the magnetic vector potential due to the cylinder current.

The fin currents at the free-space edges and at the fin-cylinder join are given by the boundary conditions

$$\vec{J}_\perp(\vec{r},t) = 0 \;,\; \vec{J}_{//}(\vec{r},t) \to \infty \qquad \text{(free-space edge)}$$

$$\frac{\partial \vec{J}_\perp(\vec{r},t)}{\partial n} = 0 \;,\; J_{//} = 0 \qquad \text{(free-cylinder join)} \quad (3\text{-}12)$$

where $\vec{J}_\perp(\vec{r},t)$ = current component perpendicular to the edge or join
$\vec{J}_{//}(\vec{r},t)$ = current component parallel to the edge or join.

This completes the solution for a target consisting of a solid with thin plates attached. It should be noted that while separate equations are used to solve for $\vec{J}_C$ on the cylinder and for $\vec{J}_F$ on the fins, the integrals in (3-2) and (3-11) over $\vec{J}$ refer to both $\vec{J}_C$ and $\vec{J}_F$ so that the equations are coupled. The marching in time procedure allows the solution by solving first (3-2)

and then (3-11) at each time step.

3.2 NUMERICAL IMPLEMENTATION

To obtain a solution of the space-time integral equations for a cylinder with fins attached, each of the components of the problem must be represented mathematically. First, the geometry of the scatterer and the characteristics of the incident field must be numerically specified. From these, the surface and fin currents can be computed using numerical representations of (3-2) and (3-11). This is accomplished by carrying out the integration and differentiation numerically and using a "marching on in time" procedure. The far-scattered field can be computed directly from the current densities by using a numerical representation of (3-4).

To describe the scatterer geometrically, the scattering surface is divided into curvilinear patches of approximately equal area with a space sample point at the center of each patch. The spacing of these sample points (and thus, the size of the patches) is chosen small enough to give both a good representation of the scatterer itself and of the currents that exist on the scatterer. The sample point spacing affects the time increment Δt at which the current densities can be calculated. The time increment must not exceed the time it takes a wave, moving at the speed of light, to travel between the closest space points. This insures that the integral equation can be expressed as a recurrence relation in time and that a matrix inversion is not necessary to obtain a solution.

The space-time integral equations represent, in principle, the solution of the scattering problem for cylinders with fins attached for an arbitrary incident field. Although the equations can be solved for each incident field separately, it is very inefficient to do so. Since in most practical scattering problems the excitation is a plane wave, a more efficient way to approach this problem is to compute the scattered response when the incident wave is an electromagnetic impulse. Once the impulse response of a target has been obtained, the response due to any incident plane wave, whose spectrum is contained within the spectrum of an impulse, can be calculated by a simple

convolution procedure. Moreover, the impulse response is intimately related to the actual geometry of the target, and thus, the potential for developing techniques to determine the impulse response of a scatterer by an inspection of its geometry is ever present.

For the numerical solution, however, it is not practical to use an ideal impulse for an excitation. Thus, in this solution a regularized or smoothed impulse is used. The form of this illumination at the origin is the Gaussian regularization of an impulse, namely

$$H^i(t) = \frac{a_n}{\sqrt{\pi}} \; e^{-(a_n t)^2}$$

which converges to a delta functional as n goes to infinity. The time domain integral equations can be solved exactly for bodies with linear dimensions up to several pulse widths of this regularized impulse. In this solution consideration is limited to bodies of this size.

The currents flowing on the cylinder and on the fin are computed using numerical representations of (3-2) and (3-11). For the purpose of discussing the numerical solution, only the x-components of these equations will be considered. Similar representations are used for the calculation of the other components.

For the numerical solution, (3-2) for the x-component of the cylinder current at sample point i and time t is represented as

$$J_{Cx}(r_i,t) = \frac{1}{(1 \pm e)} \left[2\left(n_{yi} H^i_z - n_{zi} H^i_y\right) + \frac{1}{2\pi} \sum_{\substack{\ell=1 \\ \ell \neq i}}^{N} \left\{ F(J_x) \left(r_{yi} \frac{n_{Ry}}{R} + n_{zi} \frac{n_{Rz}}{R} \right) \right.\right.$$

$$\left.\left. - F(J_y)\; n_{yi} \frac{n_{Rx}}{R} - F(J_z)\; n_{zi} \frac{n_{Rx}}{R} \right\} \Delta S_\ell \right] \qquad (3\text{-}14)$$

where

$(1 \pm e)$ = self-term correction factor for observation patch i (See Appendix 7-3)

$\left(H^i_y, H^i_y\right)$ = the y- and z-components of the incident field at patch i, time t

N = number of grid patches on the cylinder and fin

$F(J) = J\left(r_\ell,\tau\right)/R + \partial J\left(r_\ell,\tau\right)/\partial\tau$

$J_x\left(r_\ell,\tau\right)$ = the x-component of the current density at patch ℓ, time τ

$\tau = t - R$

t = time in light-meters

R = distance from the integration patch ℓ to the observation patch i: $R = \sqrt{\left(x_i - x_\ell\right)^2 + \left(y_i - y_\ell\right)^2 + \left(z_i - z_\ell\right)^2}$

$\hat{n}_{ni}$ = unit normal at patch i, $\left(n_{xi}, n_{yi}, n_{zi}\right)$

$\hat{R}$ = unit vector from patch ℓ to patch i, $\left(n_{Rx}, n_{Ry}, n_{Rz}\right)$

$$n_{Rx} = \frac{x_i - x_\ell}{R}$$

$$n_{Ry} = \frac{y_i - y_\ell}{R}$$

$$n_{Rz} = \frac{z_i - z_\ell}{R}$$

ΔS_ℓ = area of patch ℓ .

The time differentiation and interpolation necessary for the evaluation of the integrands appearing in (3-2) are performed numerically by representing the surface current with a fourth-order polynomial. In order to achieve the best accuracy, the five points used for the representation are chosen such that the current is evaluated as near as possible to the middle of them.

The numerical representation of (3-11) for the x-component of the fin current at r_i,t is obtained by representing the second time derivative of the fin current by a three-point difference approximation, yielding

$$J_{F_x}\left(r_i,t\right) = 2J_{F_x}\left(r_i,t - \Delta t\right) - J_{F_x}\left(r_i,t - 2\Delta t\right) + \frac{\Delta t^2}{\gamma_{F_i}}\left\{\epsilon\,\frac{\partial E_x^i\left(r_i,t - \Delta t\right)}{\partial t} + \frac{\partial^2 A_x}{\partial x^2} + \frac{\partial^2 A_z}{\partial x \partial z} + \frac{\partial^2 A_y}{\partial x \partial y} - \frac{\partial^2 A_{x_{NS}}}{\partial t^2}\right\} \tag{3-15}$$

where

$$\Delta t = \text{solution time step}$$

$$A_x = \gamma_{F_i} J_{F_x}\left(r_i, t - \Delta t\right) + A_{x_{NS}}$$

$$A_{x_{NS}} = \sum_{\substack{\ell=1 \\ \ell \neq 1}}^{N} \frac{J_x\left(r_\ell, \tau\right)}{R} \Delta S_\ell$$

$$\tau = t - \Delta t - R \ .$$

The space and time derivatives in (3-15) are evaluated using three- and five-point difference approximations. For the time interpolation a linear approximation is used.

The equations for the surface and fin currents are solved with a digital computer by simply marching on in time. The computation starts at a point in time before the incident field reaches the scatterer and proceeds sequentially in time in the same manner that nature would solve the problem in the real world. It is important to note that since the minimum spacing between space sample points on the surface is not less than Δt, then (3-14) and (3-15) give the current density in terms of other currents at times not later than $(t - \Delta t)$ which are already known. Thus, the integral equations (3-2) and (3-11) have been reduced to recurrence formulas in time and the need to perform matrix inversions has been eliminated.

Once the current densities have been computed, the far-scattered field can be calculated directly using a numerical representation of (3-13). For computation purposes, (3-13) is expanded in rectangular coordinates yielding

$$H_x^s(r,t) = \frac{1}{4\pi r} \sum_{\ell=1}^{N} \left(\frac{\partial J_y\left(r_\ell, \tau\right)}{\partial \tau} n_{rz} - \frac{\partial J_z\left(r_\ell, \tau\right)}{\partial \tau} n_{ry} \right) \Delta S_\ell$$

$$H_y^s(r,t) = \frac{1}{4\pi r} \sum_{\ell=1}^{N} \left(\frac{\partial J_z\left(r_\ell, \tau\right)}{\partial \tau} n_{rx} - \frac{\partial J_x\left(r_\ell, \tau\right)}{\partial \tau} n_{rz} \right) \Delta S_\ell$$

$$H_z^s(r,t) = \frac{1}{4\pi r} \sum_{\ell=1}^{N} \left(\frac{\partial J_x\left(r_\ell, \tau\right)}{\partial \tau} n_{ry} - \frac{\partial J_y\left(r_\ell, \tau\right)}{\partial \tau} n_{rx} \right) \Delta S_\ell$$

where

$$\vec{H}^s = H_x^s \hat{x} + H_y^s \hat{y} + H_z^s \hat{z}$$

$$\hat{r} = n_{rx} \hat{x} + n_{ry} \hat{y} + n_{rz} \hat{z} \ .$$

The time differentiation and interpolation necessary for the evaluation of $\partial J\ r_\ell, \tau\ /\partial\tau$ are performed numerically using a five-point Lagrange interpolation formula.

The geometry parameters used for the description of the far-scattered field are illustrated in Figure 2-1. In this sketch the incident field is shown propagating in the yz-plane and making an angle α with the z-axis. The scattered fields produced by the surface currents are then computed in the two principal planes. The scattered field is computed in the yz-plane at angles ψ_{yz} with respect to the direction of propagation of the incident wave. In this plane the two orthogonal components used to represent the scattered field are the component perpendicular to the yz-plane, $\vec{H}^s_{yzx}$, and the component tangent to the yz-plane, $\vec{H}^s_{yzt}$. The other plane in which the scattered field is computed is the px-plane, which is formed by the direction of propagation of the incident wave and the x-axis. In this plane the two components used to represent the scattered field are the component perpendicular to the px-plane, H^s_{pxp}, and the component tangent to the px-plane, H^s_{pxt}. These scattered fields are computed at angles ψ_{px}, which are measured with respect to the direction of propagation of the incident wave.

3.3 RESULTS FOR MISSILE MODEL

A sketch of the model used for calculation and measurement is shown in Figure 3-1. The dimensions are given in inches. The size of the model was chosen for convenience as L = 26.25", D = 2.5", this represents about 1/8 scale. The relative dimensions of L, D, the wings and stabilizers are close to the actual dimensions (as published in Jane's "All the World's Aircraft"). In these as in all other respects, the model closely resembles the actual missile, except for some detail not deemed of great importance to the response. The actual missile dimensions are given as L = 5.5 m and D = .53 m.

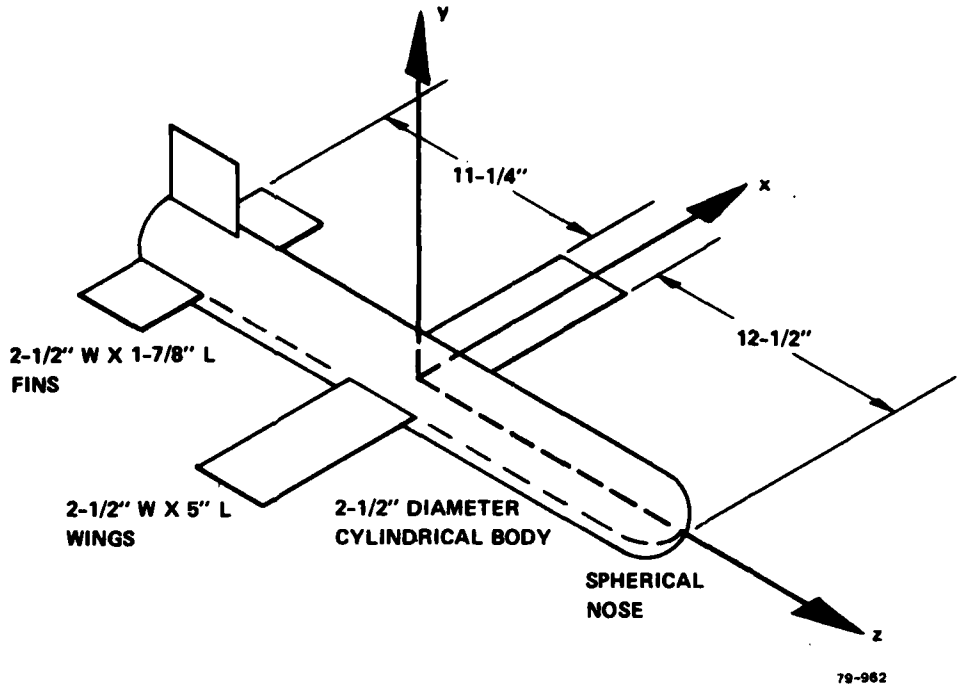

FIG. 3-1 Tomahawk model.

The computed responses are given in Figure 3-2, at several aspects from $\alpha = 0°$ (nose on) to $\alpha = 90°$ (broadside). The angle α is measured in the symmetry plane, which is the vertical plane for a horizontally flying missile.

The time scale is in units of light-inches, corresponding to the dimensions given for the model. The features of the response can thus be related directly to the physical model.

Consider the response at $\alpha = 0$. First a small doublet resembling the derivative of the imput pulse appears at $t = -25$. This is the specular response from the rounded nose. The large positive peak at $t = -2.5$ corresponds to reflection from the leading edge of the wings. The remainder of the response results from the complex interaction of wings, cylinder and the remainder of the target.

The main effect in going from $\alpha = 0$ to $\alpha = 90$ is that the above features move closer in time. Finally, at $\alpha = 90$, the specular response from the cylinder and that from the wing surface join to make a large initial response. The later bumps at $t = 6$ and $t = 12$ can be interpreted as the responses due to creep around the fuselage and the wings.

Measurements were made on the time domain scattering range for an aluminum model of the same dimensions. The results of these measurements are compared with calculations in Figure 3-3, at several angles. It is seen that the comparisons are quite good.

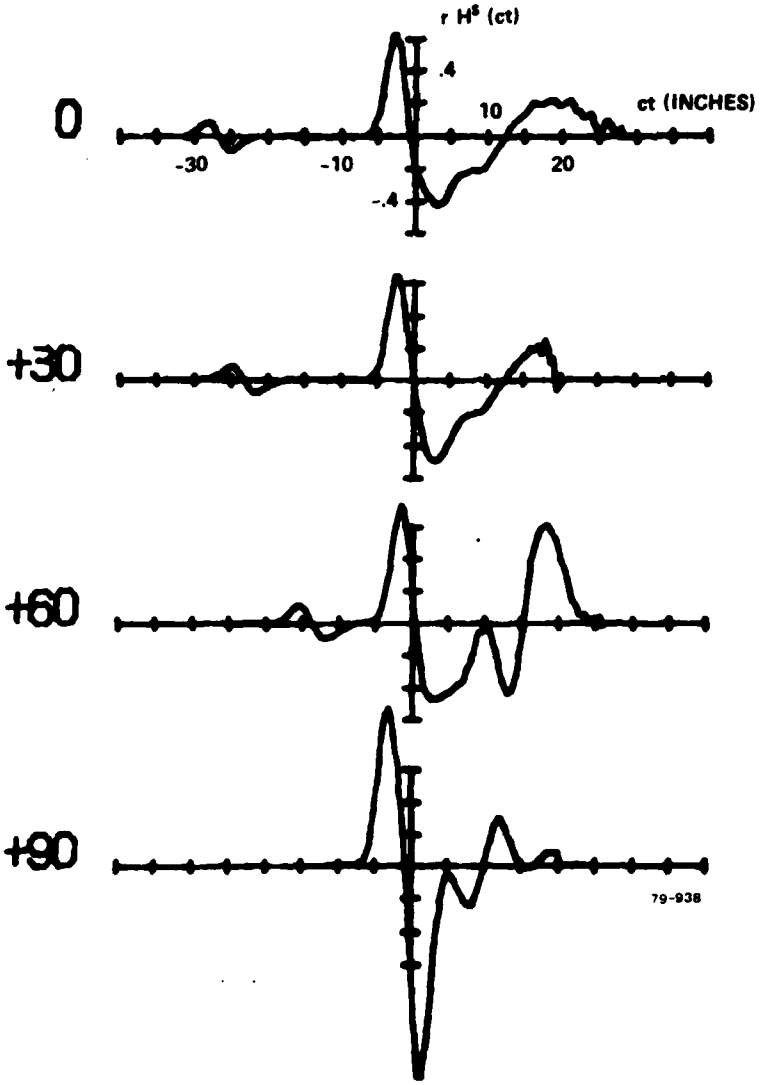

FIG. 3-2 Smoothed impulse response – Tomahawk.

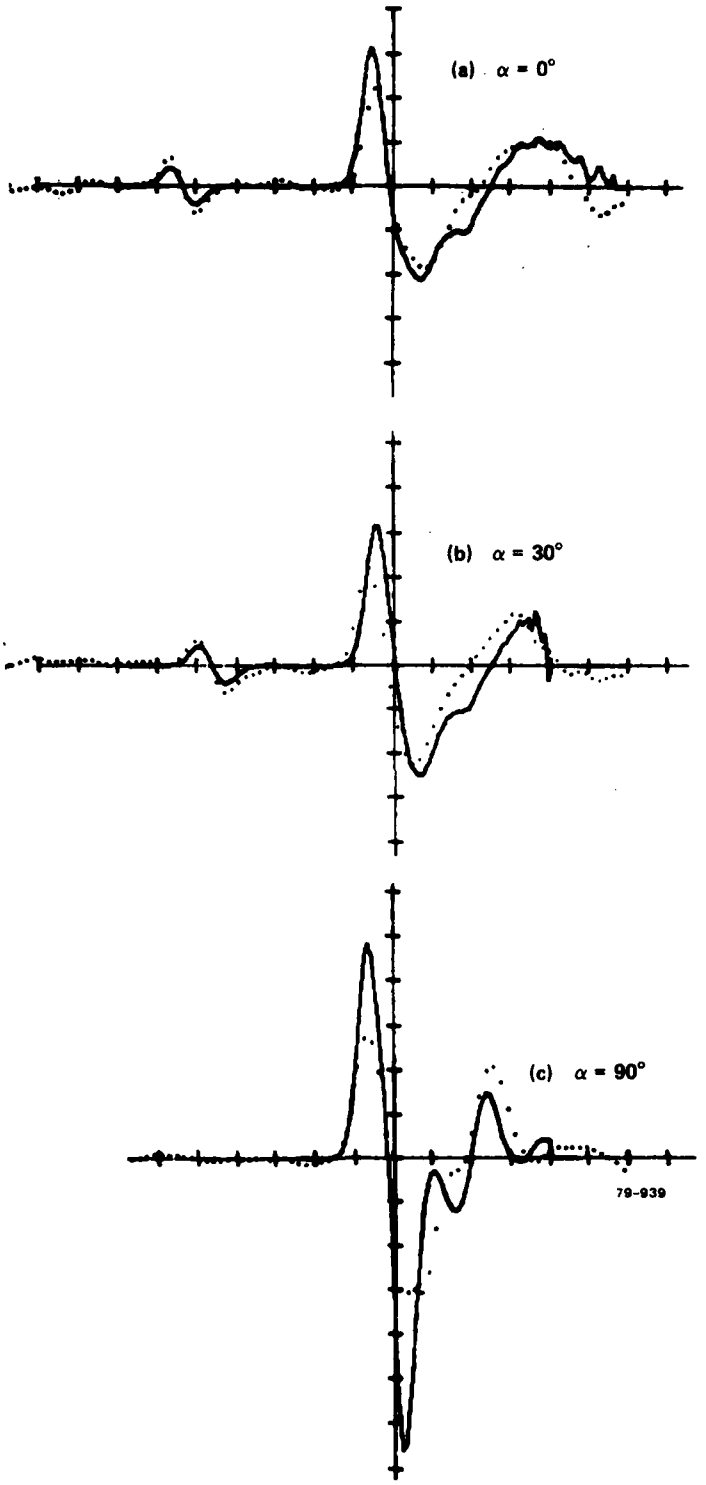

FIG. 3-3 Comparison of measured and calculated responses – Tomahawk.

SECTION IV

TIME DOMAIN MEASUREMENTS

A necessary ingredient for any successful development of techniques for the solution of previously unsolved scattering problems is the availability of actual measurements that can be used to verify the new techniques. During this effort the Sperry Research Center's Time Domain Scattering Range was used for these measurements. Section 4.1 describes, in summary form, this measurement system, its operation, and its important performance characteristics. The measurement results which were taken for this effort are described in Section 4.2.

4.1 MEASUREMENT SYSTEM

The Sperry Research Center's Time Domain Scattering Range is a system for obtaining a low-noise response in the nanosecond region. It consists of a ground plane scattering range, a step function source, a sampling oscilloscope receiver, and a laboratory instrumentation computer for control and processing. The system signal source is a high-voltage switch which generates a 300 V step function with a risetime less than 100 ps. The signal is radiated, virtually undistorted, from a vertical wire transmitting antenna located at the center of a 20 foot diameter circular ground plane. This wave illuminates the target and the resulting scattered waveform is received on a flush-mounted coaxial horn antenna, which essentially smooths and differentiates the signal and thus provides the smoothed impulse response of the target. The received waveform is sampled by a 12 GHz sampling oscilloscope that has been triggered by the initial pulse and whose sampling gate deflection is under the control of a small instrumentation computer. Unprocessed data are displayed on the oscilloscope CRT while the sampled-and-held waveform is passed through a low-pass filter, digitized, read into the computer, and stored on magnetic tape automatically. The waveforms are stored in such a way that they are ready for the subsequent operations of averaging (to remove short-term noise) and baseline processing. The effects of baseline contamination are subtracted from measured waveforms to improve system accuracy.

The time-domain scattering range provides a simple technique for obtaining transient time-domain data or multi-octave frequency-domain data. The crucial feature that the time-domain scattering range yields, is a "free time window" between the arrival of the direct wave and the arrival of unwanted reflections. Targets are usually located anywhere from two to five feet from the transmitting antenna. The response from the antenna tip and the ground plane edge occur at approximately 15 ns. Thus, a "clear window" exists between 4 ns and 15 ns which can be used to view the target responses. The entire region between the direct transmission and the range edge response forms this "free time window" for viewing the target response. The unwanted reflections are gated out in time. Thus, undistorted transient target responses can be viewed without resorting to anechoic chambers.

The accuracy of the measurement system has been estimated for the results presented in this section. The peak of the incident pulse as measured on the sampling oscilloscope is approximately 400 mV, and a typical target response has a peak value in the vicinity of 5 mV. When using the 10 mV scale on the sampling oscilloscope, the standard deviation of the sample mean is estimated to be

$$\sigma_{\bar{v}} = 0.5 \text{ mV}$$

if 16 scans are averaged. Thus, the estimated standard deviation of the sample mean $\bar{v}$ is in the vicinity of 10% of the peak value of the target response.

In addition, the measured responses are further processed by means of a convolution procedure to obtain the response due to a Gaussian shaped incident pulse rather than the approximate smoothed impulse used in the actual measurements. Figure 4-1 displays the actual measured incident pulse along with the smoothed Gaussian pulse that was used in the convolution process. The frequency spectrum of these two pulses is displayed in Figure 4-2. The time-domain expression for the Gaussian pulse is given by

$$e(t) = E_o \frac{a_n}{\sqrt{\pi}} \exp\left[-a_n^2 \left(t - t_o\right)^2\right]$$

and the frequency domain expression is

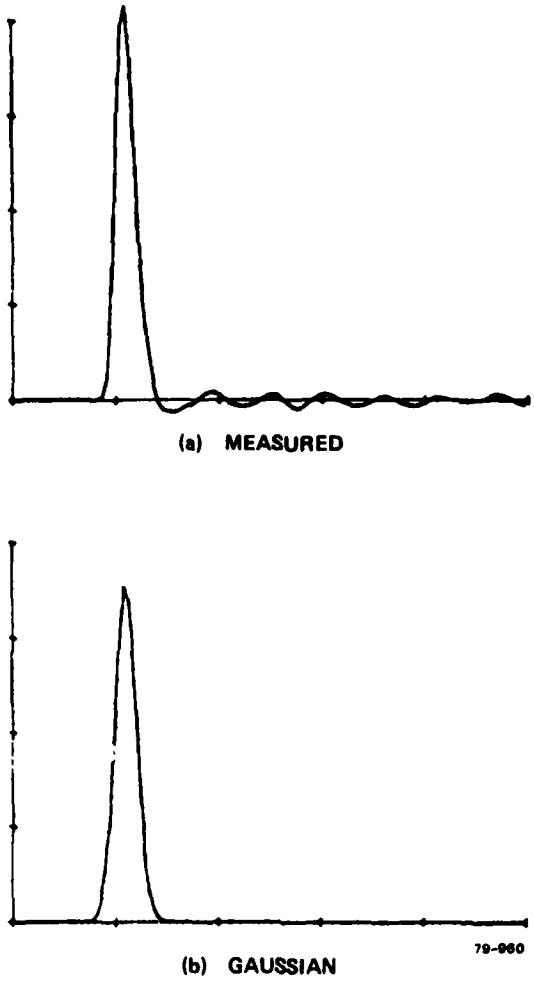

FIG. 4-1 Incident pulse (hor. scale: 0.5 ns/div.; vert. scale: 100 mV/div.).

$$E(\omega) = E_o \exp\left[-\omega^2/(2a_n)^2\right] \exp\left[-j\omega t_o\right] .$$

The amplitude coefficient E_o was set equal to the dc value of the measured incident pulse. The width coefficient a_n was obtained by requiring that the 50% value of $|E(\omega)|$ occur at the same point in frequency as the 50% value of the magnitude of the transformed measured incident pulse. The width of the resulting Gaussian pulse becomes 0.59 ns or approximately 7 inches. An added benefit of this process is the reduction of high frequency noise in the response.

This measurement system provides the capability of measuring and recording the processed smoothed impulse response data on computer computable tape. These data may then be used to find the response due to any radar waveform whose spectrum is contained within the spectrum of the original measurement smoothed impulse illumination. Futher details of this system may be found in the references [5,6].

4.2 MEASUREMENT RESULTS

In previous studies the smoothed impulse response was measured for numerous target geometries. These previous measurements are summarized in reference [6]. During the present contract, smoothed impulse responses were measured for a dielectric sphere, a dielectric sphere-capped cylinder and a dielectric right circular cylinder. The dielectric material used for the target models was nylon which has a relative permittivity of about 3 [8]. The smoothed impulse responses of the same shaped conducting targets were also measured for comparison purposes. Finally, the smoothed impulse response of the Tomahawk missile model displayed in Figure 3-1 was measured. A summary of the target geometries used for the measurements is displayed in Table I. The smoothed impulse responses which are shown in the remainder of this section are due to the incident smoothed impulse shown in Figure 4-1, which has a width $\left(\frac{4}{a_n}\right)$ of 0.59 ns and spectrum with components out to 4 GHz as shown in Figure 4-2. In viewing the measured smoothed impulse response results that are displayed in Figures 4-3 through 4-7 in the remainder of this section, it should be kept in mind that two standard deviations represent

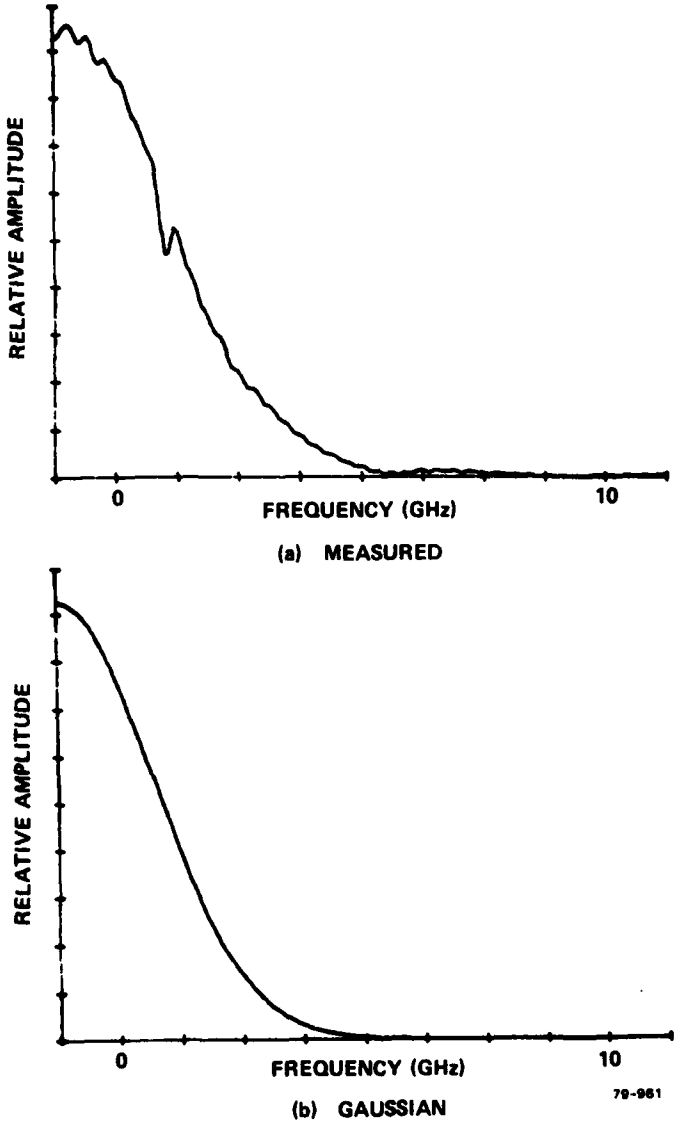

FIG. 4-2 Spectrum of incident pulse.

about 1 mV. Thus, apparent features of the waveforms that have variations less than this have less statistical significance and should be discounted.

In Figure 4-3 the measured smoothed impulse response of spherical targets is displayed. Both nylon and conducting spheres of 8" diameter and 4" diameter were measured. The first positive pulse, appearing slightly before 1 ns, is due to the specular return. This amplitude for the 4" diameter spheres is approximately half that of the 8" diameter spheres. Note also that this amplitude of the dielectric spheres is approximately one-third that of the conducting spheres. The creeping wave return is evident at $t \cong 2.5$ ns for the 8" conducting sphere and at $t \cong 1.8$ for the 4" conducting sphere. The returns from waves traveling through the dielectric spheres and being reflected from the back side are apparent at $t \cong 3$ ns for the 8" dielectric sphere and at $t \cong 2.1$ ns for the 4" dielectric sphere. The presence of baseline contamination of 1 mV and less also appears to be present at later points in time.

The measured smoothed impulse response of a nylon and a conducting sphere-capped cylinder with TE polarization are shown in Figure 4-4. The cylinder has a length of 12 inches and a diameter of 4 inches. Axial incidence corresponds to zero degrees. The target is rotated about its center for these measurements which correspond to the time $t \cong 3$ ns on this figure. The conductor responses in Figure 4-4(b) are included for completeness where the specular return, small side return, and creeping wave return can be easily discerned. The dielectric measurements displayed in Figure 4-4(a) are of low amplitude and in most cases less than 1 mV. Again, features similar to those of the conducting case may be seen in Figure 4-4(a) but other variations, especially in the 0° and 30° results later in time, may be due to some systems error.

Figure 4-5 displays the measured smoothed impulse response for both dielectric and conducting right circular cylinders with TE incidence. The cylinder has a length of 8 inches and a diameter of 12 inches. Axial incidence corresponds to zero degrees. The target is rotated about its center for these measurements which correspond to the time $t \cong 2.5$ ns on this figure. Both the dielectric and conducting results are of good quality. Again the specular return amplitude for the dielectric is approximately one-third the value measured for the conducting target. The portion of the dielectric return due to

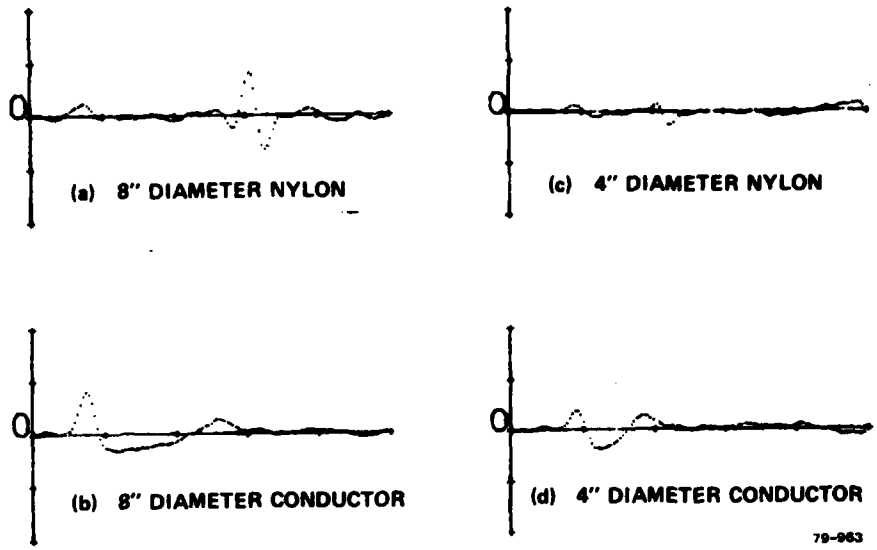

FIG. 4-3 Smoothed impulse response of spheres (hor. scale: 1.0 ns/div.; vert. scale: 5mV/div.).

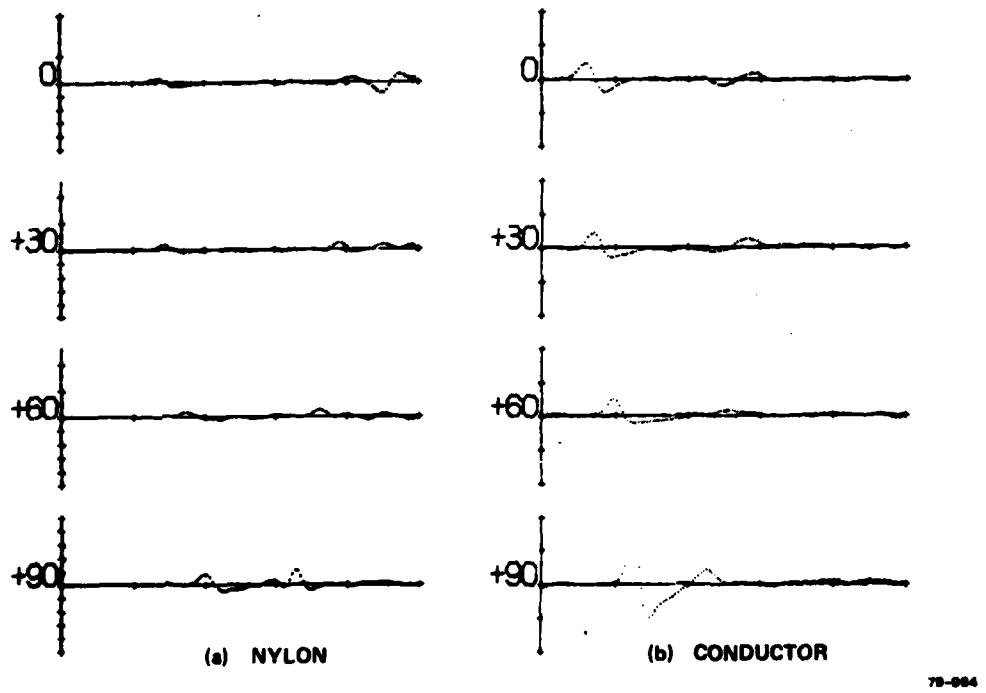

FIG. 4-4 Smoothed impulse response of sphere capped cylinder with TE polarization (hor. scale: 1.0 ns/div.; vert. scale: 5 mV/div.).

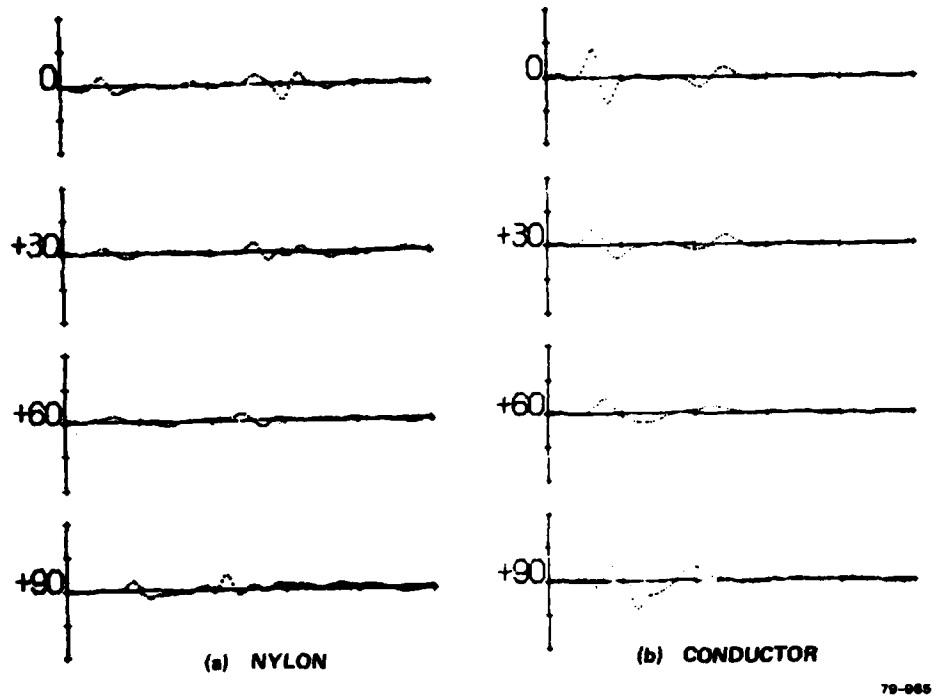

FIG. 4-5 Smoothed impulse response of right circular cylinder with TE polarization (hor. scale: 1.0 ns/div.; vert. scale. 5 mV/div.).

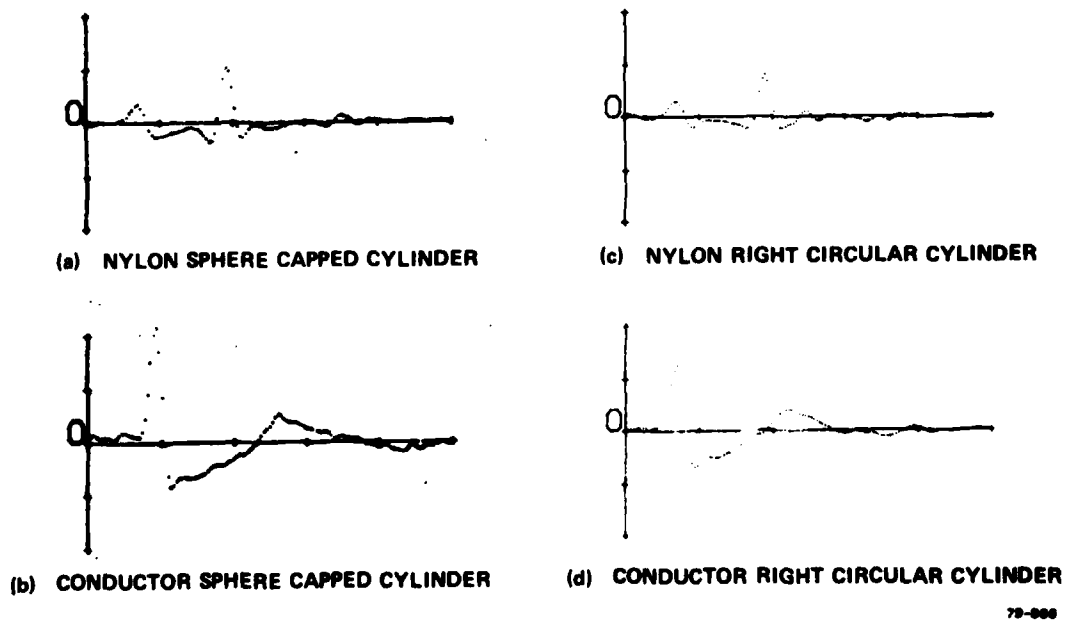

FIG. 4-6 Smoothed impulse response of cylinders with TM polarization (hor. scale: 1.0 ns/div.; vert. scale: 5 mV/div.).

wave traveling through and being reflected is more complicated than the creeping wave effects noted in the conductor. In fact, these returns in the dielectric case are probably a number of waves which have been called glory waves.

The TM responses for broadside incidence for both the sphere-capped cylinder and the right circular cylinder are shown in Figure 4-6. As before, the specular return for the dielectric target is approximately one-third of that for the conducting target. In this case, however, the internally reflected wave of the dielectric is about twice the size of the creeping wave of the conductor. It also has a more complicated structure.

Finally, Figure 4-7 displays the smoothed impulse response of the Tomahawk missile model that is sketched in Figure 3-1. Nose-on incidence corresponds to zero degrees. The target is rotated about its center which corresponds to time t $\cong$ 5 ns on this figure. Note also that the time window is 10 ns here rather than the 5 ns in the previous results. The primary returns from the nose, wings and tail region can be easily distinguished. The secondary returns from the traveling currents and interactions can also be observed.

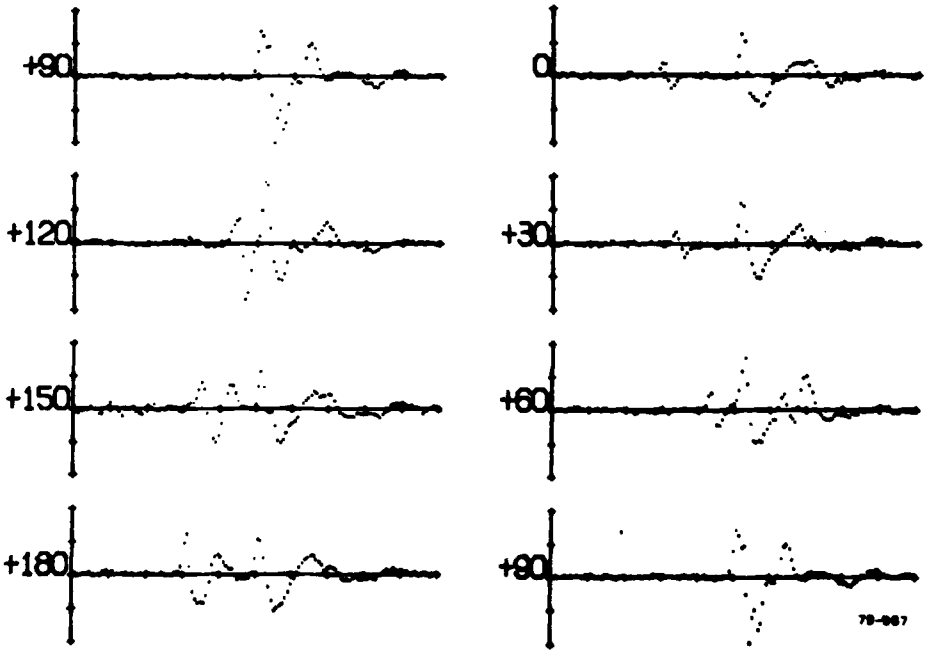

FIG. 4-7 Smoothed impulse response of Tomahawk missile model (hor. scale: 1.0 ns/div.; vert. scale: 5 mV/div.).

TABLE I

SUMMARY OF TARGET GEOMETRIES

- 8" diameter sphere
  - (1) nylon $(\varepsilon_r = 3)$
  - (2) conducting
- 4" diameter sphere
  - (1) nylon $(\varepsilon_r = 3)$
  - (2) conducting
- 4" diameter by 12" long sphere-capped cylinder
  - (1) nylon $(\varepsilon_r = 3)$
  - (2) conducting
- 4" diameter by 8" long right circular cylinder
  - (1) nylon $(\varepsilon_r = 3)$
  - (2) conducting
- Tomahawk missile model
  (see Figure 3-1)

SECTION V

SUMMARY AND CONCLUSIONS

A time domain solution was formulated and implemented for the problem of electromagnetic scattering from a dielectric solid. The approach, called the space-time integral equation approach, is applicable to bodies of any shape. The computed time domain response can be directly related to target shape. In the frequency domain the equivalent range of validity is for ka from 0 to 6 or more (well into the resonance region); techniques to extend this over the entire spectrum have been presented for conducting targets in [5]. The approach was demonstrated on a dielectric sphere and sphere capped cylinder. The solution for the dielectric sphere was verified by comparison with the known classical solution. The solution for the sphere-capped cylinder was verified by measurement. The problem of extending the solution to targets of dispersive materials was discussed.

The technique was applied to a conducting target of complex shape resembling closely a Tomahawk missile. Responses were calculated and verified by measurement. The time domain responses were shown to be highly suggestive of principal target features.

The time domain scattering range was described. Results were given for several conducting and dielectric targets at several aspects.

SECTION VI

REFERENCES

1. J.A. Stratton, Electromagnetic Theory, McGraw Hill, 1941, pp. 563-573.

2. J.J. Mikulski and E.L. Murphy, "The Computation of Electromagnetic Scattering from Concentric Spherical Structures," IEEE Trans. AP-11, March 1963.

3. J.R. Mautz and R.F. Harrington, "Electromagnetic Scattering from a Homogeneous Body of Revolution," TR-77-10, Dept. of Electrical and Computer Engineering, Syracuse University, November 1977.

4. J. Ch. Bolomey, Ch. Durix, and D. Lesselier, "Time Domain Integral Equation Approach for Inhomogeneous and Dispersive Slab Problems," IEEE Trans. AP-26, September 1978.

5. C.L. Bennett, A.M. Auckenthaler, R.S. Smith, and J.D. DeLorenzo, "Space Time Integral Equation Approach to the Large Body Scattering Problem," SCRC-CR-73-1, Sperry Research Center, May 1973; RADC-CR-73-70, AD 763794.

6. C.L. Bennett, H. Mieras, S.L. Teeter and J.P. Toomey, "Low EM Signature Response Techniques," Sperry Research Center, SCRC-CR-78-61, October 1978.

7. J.D. Jackson, Classical Electromagnetics, Wiley & Sons 1962, pp. 283-287.

8. A.M. Nicolson, et al., "Time Domain Measurement of Microwave Absorbers," AFAL-TR-71-353, Sperry Research Center, Sudbury, MA, November 1971.

9. K.S. Yee, "Numerical Solution of Initial Boundary Value Problems Involving Maxwell's Equations in Isotropic Media," IEEE Trans. Antennas and Propagation, May 1966, pp. 302-307.

10. A. Taflove, "Time Domain Solution for Electromagnetic Coupling," RADC-TR-78-142, June 1978, A056728.

SECTION VII

APPENDIX

7.1 TWO EQUATION STIE FORMULATION

A more economical formulation of the dielectric problem solution is one which utilizes only the H-field equations for the inside and outside, namely equations 2-11, 2-12 and 2-15, 2-16. Separating out the self integrations, we obtain as in Section 2.2:

$$\begin{aligned}\left(\overleftrightarrow{I} - \overleftrightarrow{\varepsilon}\right) \cdot \vec{J} + \gamma\, \hat{n} \times \frac{\partial \vec{M}}{\partial t} &= 2\, \vec{J}^{i} + \hat{n} \times \vec{I} \\ \left(\overleftrightarrow{I} + \overleftrightarrow{\varepsilon}\right) \cdot \vec{J} - \gamma\, \varepsilon_r\, \hat{n} \times \frac{\partial \vec{M}}{\partial t} &= -\hat{n} \times \vec{I}_1\end{aligned} \tag{7-1}$$

For H_n we can take the average of 2-15 and 2-16:

$$\left(1 + \frac{1}{\mu_r}\right) H_n = 2\, H_n^i + n \cdot \left[\vec{I} - \vec{I}_1\right]. \tag{7-2}$$

The system (7-1) can be solved for $\vec{J}$ and $\partial\vec{M}/\partial t$. For surface components J_u and J_v:

$$\left\{\left[1 \mp e\, \frac{\left(1 - \frac{1}{\varepsilon_r}\right)}{\left(1 + \frac{1}{\varepsilon_r}\right)}\right]\left(1 + \frac{1}{\varepsilon_r}\right)\right\}\begin{bmatrix} J_u \\ J_v \end{bmatrix} = 2\, \vec{J}^{i} + \hat{n} \times \left[\vec{I} - \frac{1}{\varepsilon_r}\, \vec{I}_1\right], \tag{7-3}$$

where $e = \gamma\,(K_u - K_v)/4$.

This is just the same equation as the first of (2-34) with $\beta = 1/\varepsilon_r$. The difference is that here we expect to obtain $\partial\vec{M}/\partial t$ by back substitution in (7-1). There is difficulty in this formulation in that the role of $\partial\vec{M}/\partial t$ in the equations is proportional to the patch radius γ.

The results of encoding this approach were poor: for some values of

ε_r obviously incorrect results were obtained, while for others the solution was unstable. It is not apparent why this was so. Since the economy of this approach was not very great it was abandoned in favor of that of Section 2.

7.2 PLANE SYMMETRY CONDITIONS

The targets that have been considered all have at least plane symmetry. Therefore the program was coded with the assumption of symmetry about the y-z plane. This reduces the amount of storage required by a factor of 2 and also reduces the computation time by a factor of 2. The incident direction is always taken in the plane of symmetry (see Fig. 2-1). The following table summarizes the symmetry conditions on the target surface. A plus sign means that the component sign is not changed upon reflection in the y-z plane; a minus sign that it does change; and a zero that the component is zero.

Quantity	TE Case x	y	z	TM Case x	y	z
$\vec{r}$	-	+	+	-	+	+
H^i	0	+	+	+	0	0
E^i	+	0	0	0	+	+
$\hat{n}$	-	+	+	-	+	+
$\vec{J}$	+	-	-	-	+	+
$\vec{M}$	-	+	+	+	-	-
H_n	scalar +			scalar -		
E_n	scalar -			scalar +		

7.3 SELF TERM INTEGRATIONS

The numerical implementation of the integral equation solution (equations 2-11 through 2-18 of Section 2.1) is made more accurate by the inclusion of terms obtained by analytic integration on the self-patch. We rederive the results of these integrations here. We will evaluate terms

of the form

$$I_S(\vec{r},t) = \frac{1}{2\pi} \oint_{\Delta S} \tau(R,\tau)\, dS' \qquad (7\text{-}4)$$

$$\tau = t - R/c$$

$$R = |\vec{r} - \vec{r}'|$$

To simplify the derivations, it is assumed that the patch is circular about $\vec{r}$ with radius γ:

$$\gamma = \sqrt{\frac{\Delta S}{\pi}} \qquad (7\text{-}5)$$

then $dS \approx 2\pi R\, d\, R$.

The self-integral of (the negative of) the first term in (2-11) is straightforward:

$$\vec{I}_{1S}(\vec{r},t) \equiv \hat{n} \times \frac{1}{2\pi} \oint_{\Delta S} \frac{1}{R} \frac{\partial \vec{M}'}{\partial t}\, dS'$$

$$= \hat{n} \times \oint_0^{\gamma} \frac{\partial \vec{M}'}{\partial t}\, dR \ .$$

Making the assumption that $\partial\vec{M}/\partial t$ is constant over the patch, we obtain:

$$\vec{I}_{1S}(\vec{r},t) = \gamma\, \hat{n} \times \frac{\partial \vec{M}}{\partial t}(r,t) \ . \qquad (7\text{-}6)$$

This result is used to rewrite equations (2-11) through (2-14), only substituting $\vec{J}$ for $\vec{M}$ in the last two. Note that $\hat{n}$ refers to the observation point $\vec{r}$.

For equations (2-15) through (2-18), we need the scalar integrals

$$N_{1S}(\vec{r},t) \equiv \hat{n} \cdot \frac{1}{2\pi} \oint \frac{1}{R} \frac{\partial \vec{M}'}{\partial t}\, dS' \ .$$

Since $\vec{M}$ lies in the surface, the quantity $\hat{n} \cdot \vec{M}(\vec{r}',t)$ is odd about $\vec{r}$. Hence

$$N_{1S} = 0 \ . \tag{7-7}$$

The remaining self integrals require some relations from differential geometry.

First consider the scalar integral

$$N_{2S} \equiv \hat{n} \cdot \frac{1}{2\pi} \oint_{\Delta S} \left(\frac{1}{R^2} + \frac{\partial}{R \partial t} \right) H_n \hat{R} \, dS' \ .$$

We need an expression for $(\hat{n} \cdot \hat{R})$, where $\hat{R} = \left(\vec{r} - \vec{r}'\right)/R$. Choose a principal coordinate system u, v; so that the Cartesian components of a point on the surface are $\vec{r} = (x(u,v), y(u,v), z(u,v))$. At observation point $\vec{r}$ define

$$\vec{r}_u = \frac{\partial \vec{r}}{\partial u} \ , \quad \vec{r}_v = \frac{\partial \vec{r}}{\partial v} \ , \quad \vec{r}_{uu} = \frac{\partial^2 \vec{r}}{\partial u^2} \ , \quad \vec{r}_{vv} = \frac{\partial^2 \vec{r}}{\partial v^2} \ .$$

(For a principle coordinate system we have that $\vec{r}_u \cdot \vec{r}_v = 0$ and $\vec{r}_{uv} \cdot \hat{n} = 0$.) $\vec{r}_u$ and $\vec{r}_v$ are surface vectors, with $\vec{r}_u \cdot \hat{n} = 0$ and $\vec{r}_v \cdot \hat{n} = 0$. The principal curvatures are defined by

$$\begin{aligned} K_u &= \left(\vec{r}_{uu} \cdot \hat{n}\right) / \left(\vec{r}_u \cdot \vec{r}_u\right) \\ K_v &= \left(\vec{r}_{vv} \cdot \hat{n}\right) / \left(\vec{r}_v \cdot \vec{r}_v\right) \ . \end{aligned} \tag{7-8}$$

$\vec{R}$ can be expanded as

$$-\vec{R} = \vec{r}' - \vec{r} = \vec{r}_u \, du + \vec{r}_v \, dv + \frac{1}{2} \vec{r}_{uu} \, du^2 + \frac{1}{2} \vec{r}_{vv} \, dv^2 + \vec{r}_{uv} \, du \, dv \tag{7-9}$$

Thus we have that

$$(\hat{n} \cdot \hat{R}) = - \frac{1}{2R} \left(K_u |\vec{r}_u|^2 \, du^2 + K_v |\vec{r}_v|^2 \, dv^2 \right) .$$

Expand

$$H_n' = H_n(\vec{r}',\tau) = H_n(\vec{r},t) + R\,\frac{\partial H_n}{\partial R} + (\tau - t)\,\frac{\partial H_n}{\partial t}$$

and assume that $\partial H_n/\partial R = 0$ and $\partial H_n/\partial t\ (\vec{r},t) = \partial H_n/\partial t\ (\vec{r}',\tau)$; then

$$\left(\frac{1}{R^2} + \frac{\partial}{R\partial t}\right) H_n' \approx \frac{H_n}{R^2}\,(\vec{r},t) \tag{7-10}$$

Taking the constant quantities outside the integral:

$$N_{2S} = -\frac{1}{4\pi} H_n \oint_{\Delta S} \frac{\left(K_u|\vec{r}_u|^2\,du^2 + K_v|\vec{r}_v|^2\,dv^2\right)}{R^3}\,dS'$$

Integrating over a circular patch of radius $\gamma = \sqrt{\Delta S/\pi}$, letting $|\vec{r}_u|\,du = R\cos\theta$, $|\vec{r}_v|\,dv = R\sin\theta$, $dS' = R\,dR\,d\theta$, we obtain

$$N_{2S} = -\frac{1}{4\pi} H_n \oint_{\Delta S} \left(K_u\cos^2\theta + K_v\sin^2\theta\right) dR\,d\theta\ .$$

Since $\int_0^{2\pi} \cos^2\theta\,d\theta = \pi$,

$$N_{2S} = -H_n\,\gamma\left(\frac{K_u + K_v}{4}\right). \tag{7-11}$$

We have used elsewhere the definition

$$e_s = \gamma\left(\frac{K_u + K_v}{4}\right). \tag{7-12}$$

The vector version of this integral is

$$\vec{I}_{2S}(\vec{r},t) \equiv \hat{n} \times \frac{1}{2\pi} \oint_{\Delta S} \left(\frac{1}{R^2} + \frac{\partial}{\partial t}\right) H_n \hat{R}\,dS' \tag{7-13}$$

Here we have to form $\hat{n} \times \hat{R}$. We see readily that $\hat{n} \times \hat{R}$ is an odd function of $\vec{r}'$. Hence

$$\vec{I}_{2S}(\vec{r},t) = 0 \qquad (7\text{-}14)$$

The last of these self integrals is

$$\vec{I}_{3S} = \hat{n} \times \frac{1}{2\pi} \oint \left(\frac{1}{R^2} + \frac{\partial}{R\partial t}\right) \vec{J}' \times \hat{R}\, dS' \ . \qquad (7\text{-}15)$$

Write J' in u,v components

$$J' = J'_u \hat{a}_u + J'_v \hat{a}_v \ ,$$

where $\hat{a}_u = \vec{r}_u/|\vec{r}_u|$, $\hat{a}_v = \vec{r}_v/|\vec{r}_v|$. Then, using (7-9):

$$\hat{n} \times \left(J'_u \hat{a}_u \times \hat{R}\right) = J'_u \frac{\hat{a}_u}{2R} \left(K_u |r_u|^2 du^2 - K_v |r_v|^2 dv^2\right) \qquad (7\text{-}16)$$

and

$$\hat{n} \times \left(\vec{J}'_v \hat{a}_v \times \hat{R}\right) = J'_v \frac{\hat{a}_v}{2R} \left(K_v |r_v|^2 dv^2 - K_u |r_u|^2 du^2\right) \qquad (7\text{-}17)$$

Again, we make the same assumptions as in (7-10) for the constancy of J, namely that $\partial J_u/\partial R = 0$ and $\partial J_u/\partial t$ = constant, so that

$$\left(\frac{1}{R^2} + \frac{\partial}{R\partial t}\right) \vec{J}' \approx \frac{\vec{J}(\vec{r},t)}{R^2} \ . \qquad (7\text{-}18)$$

The integration is similar, except that now we get a factor $(K_u - K_v)$, and moreover, this factor is of opposite sign for the $\hat{a}_u$ and $\hat{a}_v$ components. The result is

$$\vec{I}_{3S}(\vec{r},t) = e\left[\hat{a}_u J_u(\vec{r},t) - \hat{a}_v J_v(\vec{r},t)\right] \qquad (7\text{-}19)$$

where

$$e \equiv \gamma \frac{\left(K_u - K_v\right)}{4} \quad . \tag{7-20}$$

It is sometimes convenient to write this in dyadic form,

$$\overleftrightarrow{e} \equiv e\left[\hat{a}_u \hat{a}_u - \hat{a}_v \cdot \hat{a}_v\right] \tag{7-21}$$

so that

$$\vec{I}_{3S} = \overleftrightarrow{e} \cdot \vec{J} \tag{7-22}$$

The scalar version of this integral is zero because $\hat{n} \cdot \vec{J} \times \hat{R}$ is an odd function:

$$N_{3S} = \hat{n} \cdot \frac{1}{2\pi} \int_{\Delta S} \left(\frac{1}{R^2} + \frac{\partial}{R\partial t}\right) \vec{J}' \times \hat{R}\, dS' = 0 \quad . \tag{7-23}$$

MISSION
of
Rome Air Development Center

RADC plans and executes research, development, test and selected acquisition programs in support of Command, Control Communications and Intelligence (C^3I) activities. Technical and engineering support within areas of technical competence is provided to ESD Program Offices (POs) and other ESD elements. The principal technical mission areas are communications, electromagnetic guidance and control, surveillance of ground and aerospace objects, intelligence data collection and handling, information system technology, ionospheric propagation, solid state sciences, microwave physics and electronic reliability, maintainability and compatibility.